

Transpression-driven deformations of the Chočské vrchy Mountains (Western Carpathians): Insights from magnetic fabric

DOROTA STANECZEK^{1,✉}, RAFAŁ SZANIAWSKI² and JACEK SZCZYGIEL^{1,3}

¹Institute of Earth Sciences, University of Silesia, Będzińska 60, PL-41-200 Sosnowiec, Poland;

✉ dorota.staneczek@us.edu.pl, jacek.szczygiel@us.edu.pl

²Institute of Geophysics, Polish Academy of Sciences, Ks. Janusza 64, PL-01-452 Warszawa, Poland; rafsz@igf.edu.pl

³Department of Geology, University of Vienna, Althanstrasse 14, A-1090 Vienna, Austria

(Manuscript received July 5, 2021; accepted in revised form June 28, 2022; Associate Editor: Rastislav Vojtko)

Abstract: The Chočské vrchy Mts. are a part of the Tatra–Fatra Belt located in the Central Western Carpathians (Slovakia). We characterize the main Late Cretaceous–Cenozoic deformation events and the changing strain that formed the geological setting of the Chočské vrchy Mts. by applying the Anisotropy of Magnetic Susceptibility coupled with the Anisotropy of Anhyseretic Remanent Magnetization and complemented by petromagnetic analyses. We analyse Lower Cretaceous marly limestones of the Mraznica Formation (Fm.), which is a part of the Krížna nappe, and the “post-thrusting” Eocene–Oligocene Huty Fm. Petromagnetic experiments reveal that paramagnetic minerals control the magnetic susceptibility, although a distinct contribution of ferromagnetics (magnetite, hematite and likely pyrrhotite) is also documented. The magnetic fabric in both the Mraznica and Huty fms. is generally sedimentary with minor tectonic imprint. The NNE–SSW orientation of the magnetic lineation in most of the Mraznica Fm. sites corresponds well with the local bedding strike as well as the calculated regional statistical fold axis for the Krížna nappe, but it deflects from the expected orientation considering the regional Cretaceous thrusting direction. Similarly oriented magnetic lineation is also documented in some Huty Fm. sites. Magnetic and structural results reveal the dip of the post-trusting Paleogene strata covering the Chočské vrchy Mts. horst block differs from both the dip of magnetic lineation and the dip of statistical fold axis from the Krížna nappe within this uplifted block, suggesting complex uplift-related deformations. We conclude that Krížna nappe folds together with AMS lineation, both formed during Late Cretaceous thrusting, have been later rotated by an angle of 20° as an effect of Neogene transpression, which also affected the magnetic fabric of the post-thrusting cover.

Keywords: Carpathians, tectonic strain, magnetic fabrics, Anisotropy of Magnetic Susceptibility

Introduction

The Chočské vrchy Mts. are an ENE–WSW elongated mountain range located in the northern part of the Central Western Carpathians (CWC) in Slovakia (Fig. 1). This minor range is a part of the Tatra–Fatra Belt (TFB), which consists of several isolated massifs (e.g., the Malá Fatra Mts. and Tatry Mts.) that were elevated during the Neogene along SE-bounding faults (e.g., the Sub-Tatra Fault; Králiková et al. 2014a, b). Tectonic blocks forming the TFB are composed of Variscan crystalline basement with autochthonous sedimentary cover sequences overthrust by the thin-skinned Krížna and Choč nappe stacks, scarce syn-orogenic sediments (Upper Cretaceous–lowermost Paleocene facies), and the Central Carpathian Paleogene Basin (CCPB) units developed in fore-arc position behind the Outer Carpathian accretionary wedge and sealing the Paleo-alpine nappe stack (e.g., Royden & Báldi 1988; Tari et al. 1993; Soták et al. 2001; Kázmér et al. 2003; Kováč et al. 2016, 2018). The present-day tectonic setting of the study area evolved during various deformation events, which began with Variscan magmatic and metamorphic phases (Burchart 1972; Král’ 1977;

Petrík & Kohút 1997; Kohút et al. 1999; Anczkiewicz et al. 2015). The next stage, Alpine Late Cretaceous nappe stacking and related folding with a synchronous burial of the crystalline basement, was followed by Paleocene to Early Eocene exhumation and successive burial beneath the CCPB followed by final Neogene exhumation processes (Plašienka et al. 1997; Froitzheim et al. 2008; Danišák et al. 2011; Prokešová et al. 2012; Králiková et al. 2014b, 2016; Castelluccio et al. 2016).

The Chočské vrchy Mts. are bound on the south by an ENE–WSW trending Choč–Subtatric Fault (e.g., Gross et al. 1994), along which the folded Paleo-alpine nappes were elevated in the Neogene, leading to the formation of an asymmetric, northward-tilted horst structure (Kováč et al. 1994; Králiková et al. 2014b). On the north, the rocks of the nappe structure are discordantly overlain by the transgressive basal conglomerates of the Borové Fm. followed by other mostly flysh-like sediments of the CCPB.

The multi-stage tectonic evolution of the TFB has been extensively studied applying magnetic anisotropy methods. Results from several TFB massifs document tectonic overprint of magnetic fabric related to Late Cretaceous

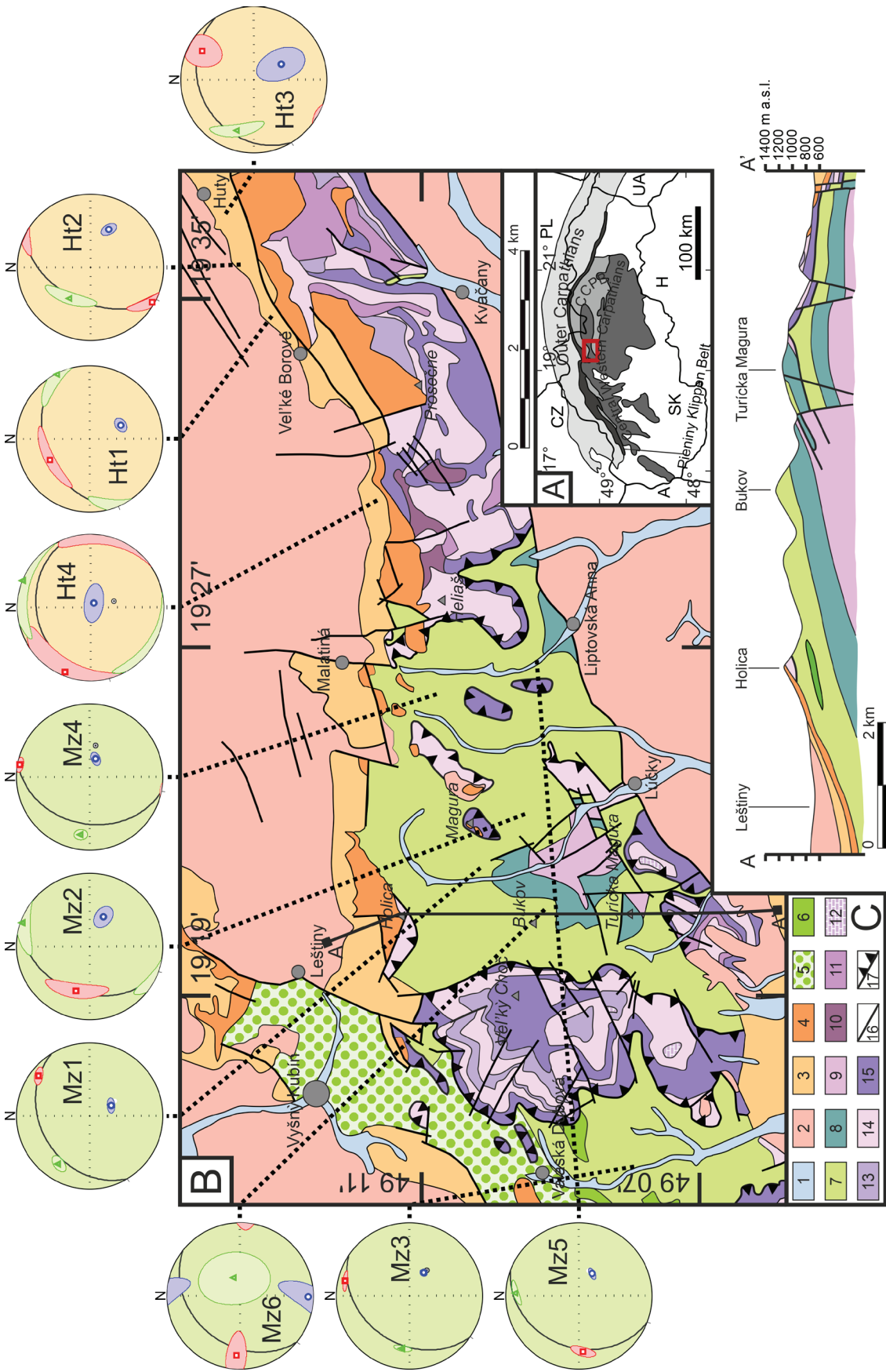


Fig. 1. Simplified geological map of the Choč Mts. with marked sampling locations, cross-sections and AMS results (B, after Gross et al. 1994). AMS plots show the k_{MAX} , k_{NIP} and k_{MIN} mean principal axes and their 95 % confidence ellipses. The grey circle shows site-mean bedding with the corresponding pole to bedding; A — Schematic map of the study area (red rectangle, Sentpetery 2011). Map explanation (C): 1 – Quaternary fluvial sediments, 2 – Zuberec Fm., 3 – Huty Fm., 4 – Borové Fm. (2 – 4 Central Carpathian Palaeogene Basin), 5 – Poruba Fm., 6 – Pármica Mb, 7 – Mraznica Fm., 8 – Jurassic sediments, 9 – Triassic sediments (5–9 Križna nappe), 10 – Hauptdolomit, 11 – Lunz Fm., 12 – Raming and Wetterstein limestones, 13 – Reifling limestones and Parthnach beds, 14 – Ramsau dolomites, 15 – Gutenstein limestones and dolomites (10–15 Choč nappe), 16 – major faults, 17 – thrust faults.

compression recorded both in the Krížna nappe and autochthonous sedimentary cover as well as in the crystalline basement (Hrouda 1983, 1986; Hrouda et al. 1983, 2002, 2018; Hrouda & Hanák 1990; Hrouda & Kahan 1991; Hrouda & Potfaj 1993; Hrouda & Vozár 1995; Grabowski 1995, 1996, 1997; Grabowski et al. 2009; Gregorová et al. 2009; Szaniawski et al. 2012, 2020). Interestingly, the orientation of tectonic fabric within individual massifs of the TFB is mostly uniform, but it seems to differ slightly between the separate massifs. This observation was explained as the effect of the different tilting and rotations of rigid horst-blocks resulting from transtensional deformation related to the Neogene inversion (Hrouda et al. 2002). In the case of Upper Eocene to Oligocene sediments, magnetic anisotropy studies revealed both purely sedimentary fabrics as well as distinct tectonic overprint. The latter was primarily detected in marginal parts of the CCPB, in the vicinity of elevated blocks of the TFB and close to the Pieniny Klippen Belt (Hrouda & Kahan 1991; Hrouda et al. 2018; Madzin et al. 2021).

Unlike most other massifs that form the TFB, there are no magnetic anisotropy results from Mesozoic rocks of the Chočské vrchy Mts. (except for one location in the westernmost margin of this unit where Kruczyk et al. (1992) only mentioned the low magnetic anisotropy of Jurassic carbonates from the Krížna nappe). The Chočské vrchy Mts. seem to be particularly interesting as this unit differs slightly from other TFB massifs due to its narrow shape (the Mesozoic rocks outcrop belt at its narrowest point does not exceed the width of 2 km). In these studies, we fill the gap presenting magnetic anisotropy results from the Chočské vrchy Mts. aiming to evaluate the Late Cretaceous–Cenozoic tectonic evolution of the area. In our studies we apply state-of-the-art laboratory techniques including, apart from standard AMS methods, advanced petromagnetic studies (quantification of IRM coercivity components) and modern research on remanence anisotropy (sub-fabrics separation based on coercivity), which have not been used so far in the studies of the northern part of the Central Western Carpathians.

In order to obtain the most readable image reflecting the course of the local tectonic evolution, we studied two formations from different tectonic units: The Lower Cretaceous marly limestones of the Mraznica Formation (Fm.) from the Krížna nappe (Gross et al. 1993) and the Eocene–Oligocene Huty Fm. (Zakopane beds in Polish terminology; e.g., West-walewicz-Mogiliska 1986) belonging to the CCPB (e.g., Soták et al. 2001; Fig. 2). Comparing the Krížna nappe and CCPB allows us to better decipher subsequent separate tectonic phases that affected rocks forming the Chočské vrchy Mts.

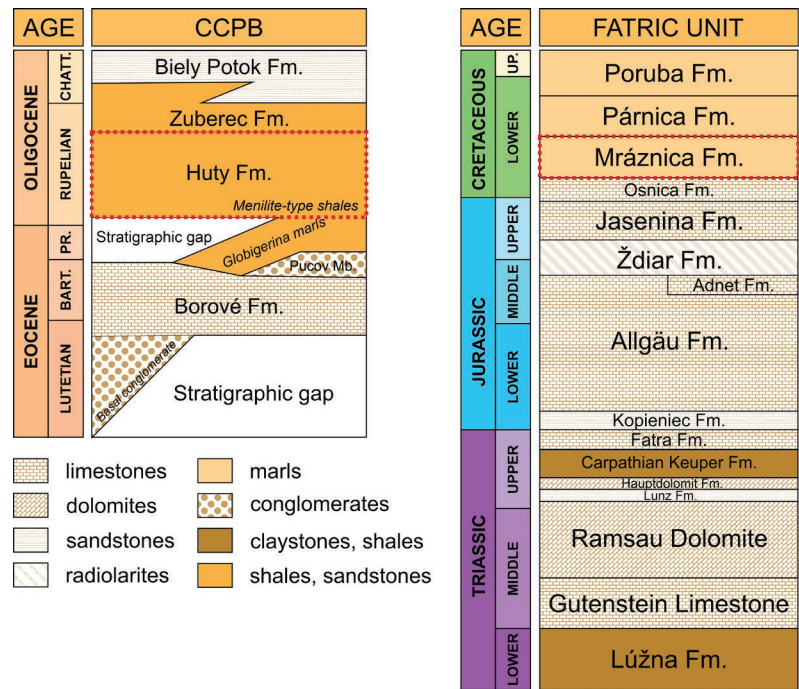


Fig. 2. Lithostratigraphic columns of the Central Carpathian Paleogene Basin units and the Krížna nappe in the Chočské vrchy Mts. modified after Gross et al. (1984), Starek (2001) and Lexa et al. (2000).

and add the obtained results to the current state of knowledge of the Carpathian tectonic evolution.

Geological setting

The Central Western Carpathians represent a fold-and-thrust belt that originated during the Jurassic–Neogene collision of the North European Platform, Adria- and Europe-derived units (Plašienka et al. 1997; Csontos & Vörös 2004; Castellucio et al. 2016; Kováč et al. 2018; Plašienka 2018). A distinctive structure present in the northern part of the CWC is the Tatra–Fatra Belt, which forms a SW–NE-oriented chain consisting of exhumed massifs built up by Paleozoic–Mesozoic rocks and separated by intramontane depressions filled with Cenozoic sediments (Andrusov 1968; Bac-Moszaszwili et al. 1979; Hrouda & Kahan 1991; Plašienka et al. 1997; Jurewicz 2005; Králiková et al. 2014a,b; Anczkiewicz et al. 2015).

The depositional age of the sedimentary succession in the Krížna nappe ranges from Lower Triassic to Late Cretaceous (e.g., Prokešová et al. 2012; Fig. 2). The Krížna nappe sedimentary succession in the Chočské vrchy Mts. includes Triassic–Lower Cretaceous sediments represented mostly by carbonatic rocks along with a few clastic units (Gross et al. 1994). The studied Mraznica Fm. consists of marly limestones with cherts passing into marls and shales (Gross et al. 1994) and subsequently to calcareous siltstones, marls, and

limestones of the Párnica Fm. (Józsa et al. 2016). The Křížna nappe exhibits both brittle and ductile deformation related to the nappe emplacement event (Plašienka & Prokešová 1996; Prokešová et al. 2012). The Choč nappe is predominantly composed of Triassic carbonates. In the eastern part of the study area, the Choč nappe forms sub-horizontal thrust sheets, while in the western part, due to erosional processes, it tends to form scarce klippen on top of the Křížna nappe (Kováč & Filo 1992; Gross et al. 1994). The NW-directed movement of the Křížna nappe started in the Early Albian, and the final emplacement terminated in the Late Turonian (Plašienka 2002; Prokešová et al. 2012). Some models assume that the thrusting of the Choč nappe in the northern part of CWC lasted until the end of the Late Cretaceous (Havrila 2011).

Paleocene exhumation exposed Mesozoic carbonate rocks to intensive weathering and karstification until the Early Eocene (Gross et al. 1980; Činčura 1990, 2002; Kováč et al. 1994, 2016; Plašienka 1997; Danišik et al. 2010; Králiková et al. 2014b, 2016; Vojtko et al. 2016). Pre-Paleogene structures are overlain by Eocene–Lower Miocene sediments of CCPB (e.g., Soták et al. 2001). After the deposition of transgressive breccias, conglomerates, and detritic limestones of the Borové Fm., the sedimentation changed from mainly carbonate to exclusively clastic, reflecting continuous basin deepening (Gross et al. 1984, 1993; Soták et al. 2001). The Huty Fm. (Eocene–Oligocene) consists of two slightly different facies: Menilite-type claystone and calcareous claystone intercalated with turbiditic sandstones (Gross et al. 1993; Soták et al. 2001). Two following facies, the Zuberec and Biely Potok fms., record the rising sedimentary supply, manifested by an increasing volume of sandstones in the succession (Gross et al. 1994; Starek et al. 2000; Soták et al. 2001).

Lower Miocene compression with the orientation of principal compressional stress axis in NW–SE direction triggered the termination of CCPB and caused a subsequent basin inversion (Kováč et al. 1994; Plašienka et al. 1997; Pešková et al. 2009; Vojtko et al. 2010). Accelerated exhumation associated with tilting of TFB massifs started in the Middle Miocene (Burchart 1972; Král 1977; Králiková et al. 2014a,b; Pešková et al. 2009; Vojtko et al. 2010). The uplift of the Chočské vrchy Mts. probably occurred along a reactivated southern extension of the Choč-Subtatric Fault, which bounds the Chočské vrchy Mts. massif from the internal, southern site (Fig. 1; Gross et al. 1993). The horst structure of the Chočské vrchy Mts. most likely formed 15–8 Ma ago (Králiková et al. 2014b). The CCPB sediments that cover the Mesozoic nappes on the north side are characterized by a moderate northward dip that seems to correspond to the inclination of the Chočské vrchy Mts. horst structure (see cross-sections in Gross et al. 1994). During the Cenozoic, the research area experienced mostly brittle deformation events (Pešková et al. 2009) while long-wavelength, asymmetric synclines of the Orava and Podhale basins were formed as a response to exhumation of the Chočské vrchy Mts. and Tatry Mts. horsts.

Methods and sampling

Sampling sites

The sampling locations have been selected with the aim of obtaining results representative of regional tectonic interpretations. All sampling sites for magnetic analysis were precisely inspected, paying special attention to deformations – outcrops with extensive local tectonic deformation (e.g., thrusts, faults, or tight folds) have been excluded from further investigation. Rocks of the Mraznica Fm. were collected in six sampling sites located along the outcrop belt of this unit in the central part of the Chočské vrchy Mts. A total of 38 hand samples were taken in the outcrops and then drilled in laboratory to give 147 standard cylindrical paleomagnetic specimens of inch diameter. All sampled rocks of the Mraznica Fm. represent grey to dark grey marly limestones.

We collected rocks of the Huty Fm. in four sampling sites situated rather close to the Mesozoic units for the best possible recognition of deformations associated with uplift of the Chočské vrchy Mts. horst. When selecting the sampling sites, we avoided coarser-grained sandstones of the Huty Fm., which most likely have distinct sedimentary magnetic fabrics associated with mineral alignment due to turbidite currents. We assumed that in such rocks the tectonic overprint would be less readable than in fine grained sandstones and mudstones deposited in lower energy sedimentary environment. Rocks of this type are commonly used for tectonic analyses based on magnetic anisotropy, and the results of several studies confirm that their magnetic fabric reflects well even a very weak deformation (e.g., Aubourg et al. 2004; Mazzoli et al. 2012; Parés 2015). Accordingly, samples were taken from the most fine-grained rocks possible but excluding highly fissile shales from which cylindrical specimens could not be drilled in the laboratory. Rocks of the Huty Fm. were collected from four sampling sites with a total of 19 hand samples, from which 72 specimens were drilled in the laboratory. In sites Ht1, Ht2, and Ht3 samples represent medium to dark grey shales and siltstones, while in Ht4, light grey silty sandstones. All specimens were oriented according to the AGICO Inc. orientation standards (<https://www.agico.com/downloads/documents/agicoprints/orpar.pdf>).

Magnetic methods

High-temperature methods

To determine the magnetic mineralogy of the rocks in this study, petromagnetic investigations were conducted, which began with thermal demagnetization of the three-component IRM (Isothermal Remanent Magnetization; Lowrie 1990) for six samples from the Mraznica Fm. and four from the Huty Fm. Measurements were conducted using a 2G SQUID cryogenic magnetometer (2G Enterprises, USA), an MMTDSC thermal demagnetizer (Magnetic Measurements, UK), and an MMPM10 pulse magnetizer (Magnetic Measurements,

UK). Each sample was magnetized along three orthogonal axes (x : 0.15 T, y : 0.5 T, and z : 3.0 T) and gradually demagnetized up to temperatures reaching 650 °C.

Temperature-dependent susceptibility measurements were performed using a KLY-5a Kappabridge with a CS4 high-temperature unit and a KLY-3 Kappabridge with a CS3 unit (Agico Inc., Czech Republic). Susceptibility variations were measured up to 700 °C with the 300 Am⁻¹ field intensity and 875 Hz field frequency. Three samples from each site were chosen for this measurement. Additionally, the ratio of ferromagnetic and paramagnetic components was calculated with Cureval8 software, applying Hrouda et al. (1997) and Chadima & Hrouda (2012) methods.

Room-temperature methods

For Isothermal Remanent Magnetization (IRM) acquisition measurements, four samples from the Mraznica Fm. and two samples from the Hutý Fm. were selected. Samples were magnetized in fields reaching 3T using a PAM1 unit (Agico Inc., Czech Republic) for low applied fields (reaching 15 mT) and an MMPM10 pulse magnetizer (Magnetic Measurements, UK) for higher fields. Remanence at 28 steps of IRM acquisition was measured using a 2G SQUID cryogenic magnetometer (2G Enterprises, USA). Afterward, IRM acquisition curves were analysed following Kruiver et al. (2001) method, which is based on cumulative logarithm Gaussian analysis. This method enables the calculation of the magnetic properties of IRM components and thus the identification of ferromagnetic minerals in a sample. Three parameters that can be determined are the saturation (SIRM), the dispersion of the distribution (DP) and the field at which half of the saturation is reached ($B_{1/2}$). Additionally, the percentage of each IRM component was calculated.

Hysteresis loop and back-field experiments were performed with a Princeton Instruments Micro-Mag vibrating sample magnetometer for 22 samples from the Mraznica and Hutý fms. The weight of each sample did not exceed 0.02 g. Every sample was demagnetized prior to the hysteresis loop experiments. All hysteresis loops started at zero applied field. The slope correction for paramagnetic minerals was applied at 70 % of the highest field (1T).

To obtain AMS data, standard-sized cylindrical specimens were measured using both MFK1 and KLY-5a Kappabridges (Agico Inc., Czech Republic) with an 875 Hz operating frequency and a 700 Am⁻¹ field intensity. The AMS ellipsoid was calculated for each measured specimen along with several quantitative parameters (K_m – mean susceptibility, P_j – corrected degree of anisotropy, T – shape parameter, L – degree of magnetic lineation, and F – degree of magnetic foliation; Jelínek 1977) using Anisoft5 software. A total of 147 specimens from the Mraznica Fm. and 72 from the Hutý Fm. were examined.

Additionally, to recognize the preferred orientation exclusively of ferromagnetic minerals in the analysed rocks, Anisotropy of the Anhyseretic Remanent Magnetization (AARM)

measurements was performed. Standard-sized cylindrical specimens were examined with a JR-6A automatic spinner magnetometer and a LDA5 unit (Agico Inc., Czech Republic). Specimens were magnetized in 12 different directions in alternating current fields (AC) reaching 150 mT or 120 mT for the Hutý Fm. and Mraznica Fm., respectively. Additionally, to distinguish and separate sub-fabrics carried by magnetic minerals with different coercivity, the Anisotropy of partial Anhyseretic Remanent Magnetization (ApARM) measurements were conducted in 0–40 mT AC for all sites, 90–150 mT for the Hutý Fm. and 90–120 mT for the Mraznica Fm. During each magnetization step a 500 μ T direct field (DC) was applied. All AARM ellipsoid parameters were calculated by Anisoft5 software.

Structural analysis

For a better, in-depth interpretation of magnetic data and to link them with the tectonic evolution of the study area, we conducted supplementary basic structural analyses. First, an attempt was made to estimate the northward tilt angle of the Chočské vrchy Mts. asymmetric horsts formed because of the Neogene exhumation. As in the case of estimations of the tilt angle of the Tatry Mts. horst (Sperner et al. 2002; Ludwiniak & Rubinkiewicz 2006; Jurewicz 2012; Szaniawski et al. 2012, 2020), in this study, we used the orientation of CCPB sediments that cover the Mesozoic nappes on the external, northern side. Orientations of the Hutý Fm. and additionally Zuberec Fm. and Borové Fm. in the area up to 2 km north of the Mesozoic units were collected during field investigations and derived from geological maps of the Chočské vrchy Mts. (both digital and paper versions; <http://apl.geology.sk/gm50js/>; Gross et al. 1994).

Afterwards we performed calculations of the statistical fold axis for the Mesozoic Mraznica Fm. using the π -pole method (best-fit great circle method; Ramsay & Huber 1987; Fossen 2010). After obtaining the statistical fold axis all previously analysed data were rotated by an angle calculated from the CCPB units which characterize the average tilting angle of the Chočské vrchy Mts.' horst. As a result, a pre-Neogene (pre-tilting) orientation of the statistical fold axis of the Mraznica Fm. sediments was obtained. All calculations were performed using InnStereo Beta 6 software (<https://innstereo.github.io/>)

Results

High-temperature methods

Thermal demagnetization of the three-component IRM

The results of thermal demagnetization of a three-component IRM are mostly consistent in the Mraznica Fm. samples and document the dominance of the soft component, presumably carried by magnetite (maximum unblocking temperature

of ~585 °C; Fig. 3a; Lowrie 1990), with much lower contribution of the hard and intermediate fractions. Only samples from sites Mz4 and Mz5 (Fig. 3b) display different behaviour, showing in addition to magnetite the significant content of the high coercivity fraction characterized by a maximum unblocking temperature of 650 °C, interpreted as hematite. Additionally, in many samples, small drops in the signal are observed at approximately 300–325 °C on intermediate and low coercivity curves which could be interpreted as a minor iron sulphides contribution.

The obtained results for the Huty Fm. samples are coherent (Fig. 4a, b) and similarly to the Mraznica Fm. show the dominance of soft component (magnetite). In the Huty Fm. magnetization values of intermediate and hard components are much lower than soft component. Most of the studied specimens also show some drops in signal intensity at 300–325 °C on intermediate and low coercivity curves indicating that in addition to magnetite, they contain some magnetic iron sulphides.

Thermal variations of susceptibility

The obtained thermomagnetic curves for the Mraznica Fm. samples (Fig. 3c, d) are characterized by low initial susceptibility values and reveal a tendency towards a hyperbolic decrease in temperatures up to 400 °C which is characteristic for paramagnetic minerals. A fast increase of susceptibility above 400 °C is related to the formation of new ferromagnetic minerals as a result of thermochemical alterations. Further drop of susceptibility at 540–580 °C documents that the newly formed mineral is magnetite.

All thermomagnetic curves for the Huty Fm. are coherent and similar to those obtained for the Mraznica Fm. samples (Fig. 4c, d). In most sites, a hyperbolic decrease in the susceptibility up to 400 °C (Fig. 4d) is visible, followed by an abrupt increase of the susceptibility which is significantly higher than that recorded in the Mraznica Fm. samples. Overall, the results from both Mraznica and Huty fms. are rather similar and document that the magnetic susceptibility is mostly controlled by paramagnetic minerals with minor contribution of ferromagnetic minerals.

Room-temperature methods

IRM acquisition curves

In most of the studied specimens from the Mraznica Fm. the IRM acquisition curves are similar and characterized by a fast increase in magnetic remanence up to 200–300 mT, followed by a relatively rapid flattening of the curve (Fig. 5) and then only minor increase of magnetic remanence values up to fields of 3T. This documents that these samples contain predominantly low to middle coercivity magnetic minerals with much lower content of higher coercivity fraction. One studied specimen from site Mz5 shows somewhat different behaviour. Here, after a rapid increase of the IRM value in the low fields, the curve does not flatten completely but

shows a distinct linear increase up to 3T. This indicates the coexistence of low and medium coercivity fractions with a significant content of high coercive minerals, presumably hematite.

Like most of the Mraznica Fm. specimens, the IRM acquisition curves for the Huty Fm. show a fast increase in magnetic remanence in fields up to 500–600 mT, after which the magnetization curve shows an almost flat, horizontal course with a very modest increase of magnetization. Magnetic remanence values acquired after applying a 3T field were higher for the Huty Fm. specimens than for the Mraznica Fm. specimens, which can be a sign of higher amounts of ferromagnetics in the first unit.

An IRM component analysis (Kruiver et al. 2001) allowed us to distinguish three components of IRM for both the Mraznica Fm. and the Huty Fm. specimens (Table 1). In the Mraznica Fm. specimens SIRM and $B_{1/2}$ values for the first, low-coercivity component reach 17 mA·m⁻¹ and 19.95 mT, respectively. The second component is characterized by homogeneous $B_{1/2}$ values (~50 mT), usually the highest percentage contribution to IRM (35–79.1 %) and SIRM values vary from 20 to 110 mA·m⁻¹. The third component exhibits the highest $B_{1/2}$ values (thousands of mT), while the SIRM values are generally quite low, with the exception of the sample from the Mz5 site where the contribution of the high coercive component is greater.

In two analysed specimens in the Huty Fm. the low-coercivity IRM component is characterized by low SIRM and $B_{1/2}$ values (up to 12 mA·m⁻¹ and up to 10 mT, respectively). The second component covers 85.5–90.3 % of IRM and it shows relatively high SIRM values (up to 200 mT). The third component resembles the highest $B_{1/2}$ values (316.2 mT and 1000.0 mT) but its contribution to IRM is generally low (up to 9.3 %).

The features mentioned above enabled us to identify PSD magnetite as a soft magnetic phase (first component in both units), SD magnetite, presumably with a small contribution of magnetic iron sulphides (second, most common component in both units). The third component present in the Mraznica Fm. and the Huty Fm. samples can be associated with hematite.

Hysteresis loop and back-field experiments

In all Mraznica Fm. samples hysteresis loops were indicative of the dominance of paramagnetic phase showing increasing and nearly linear trend with magnetization (M) up to 16.8 mA·m⁻¹·kg⁻¹ in field 500 mT. After correction for paramagnetic minerals the remanent magnetization value (M_r) does not exceed 90.6 μ Am²·kg⁻¹ (Figs. 3e, f, 4e, f; Table 2), while the saturation magnetization (M_s) varies from 325.7 μ Am²·kg⁻¹ to 1070.00 μ Am²·kg⁻¹. The ferromagnetic phase is characterized by relatively low coercivity as the mean coercivity (H_c) value was 6.0 mT while the remanence coercivity (H_{cr}) obtained in the back-field experiment reached an average value of 21.3 mT. The ferromagnetic contribution to the total magnetic susceptibility is rather low (a maximum

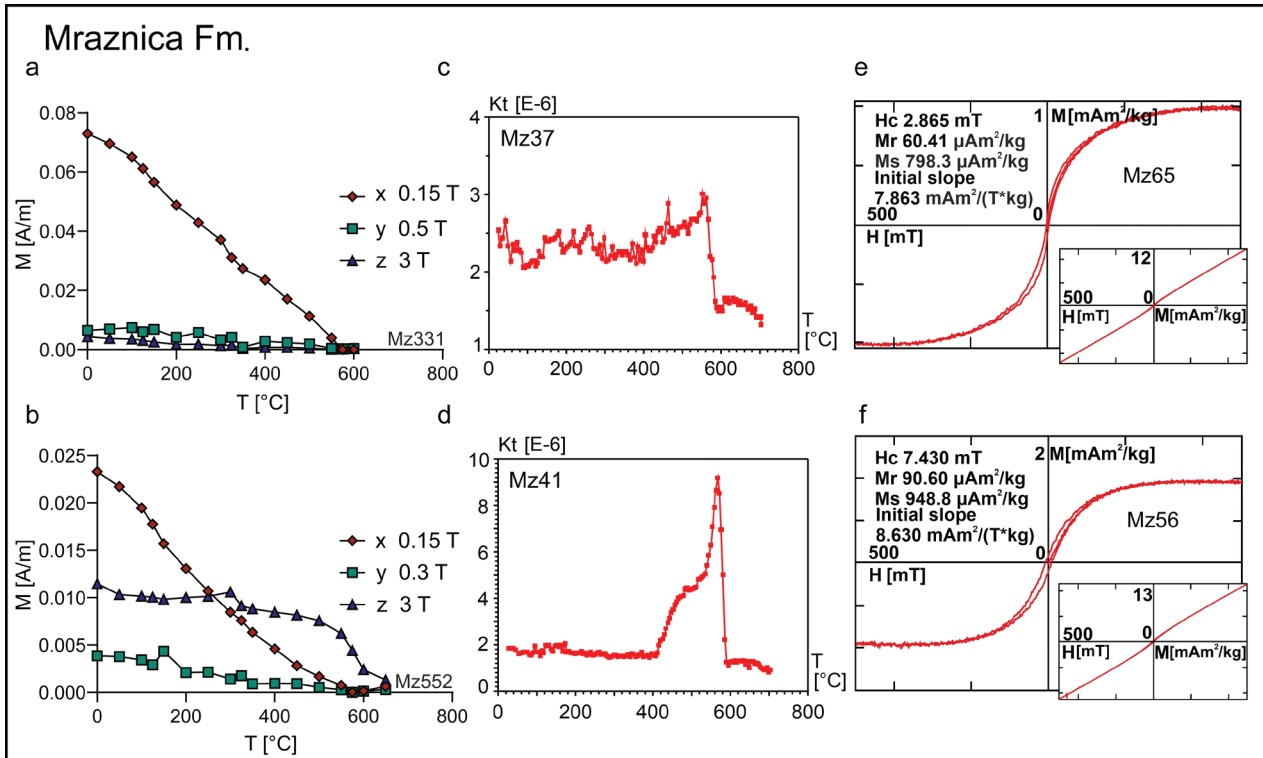


Fig. 3. Results of petromagnetic experiments of the Mraznica Fm.: **a, b** — Thermal demagnetization of a three-component IRM; **c, d** — Susceptibility monitored during heating; **e, f** — Hysteresis loops (small diagram shows the results before paramagnetic slope correction).

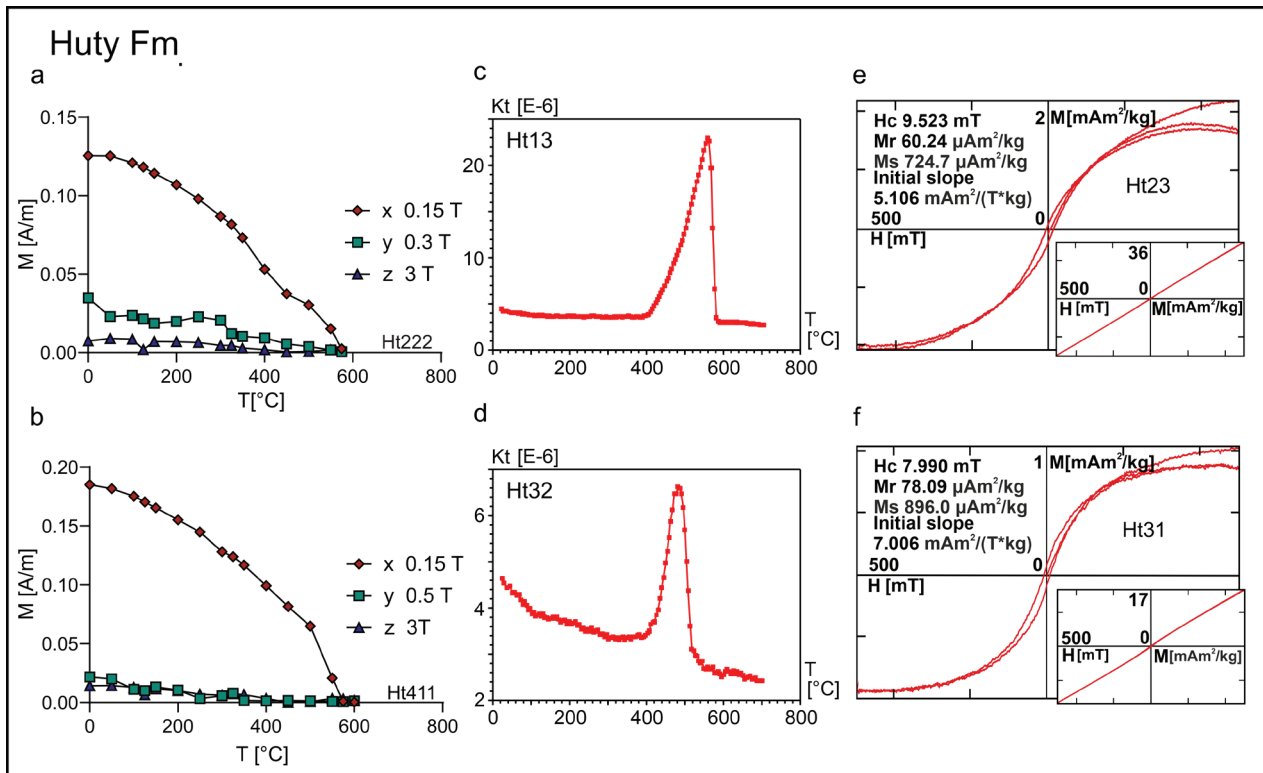


Fig. 4. Results of petromagnetic experiments for the Hutý Fm.: **a, b** — Thermal demagnetization of a three-component IRM; **c, d** — Susceptibility monitored during heating; **e, f** — Hysteresis loops (small diagram shows the results before paramagnetic slope correction).

of 33.8 %). In general, the obtained results document relatively coherent values of all parameters (Table 2).

The results for the Huty Fm. are also indicative of dominance of paramagnetic phase and quite homogenous. Therefore, the differentiation of parameter values at the site level is comparable (Table 2). Uncorrected hysteresis loops are nearly linear, and the magnetization value (M) varies from 15.4 to 56.4 $\text{mA}\cdot\text{m}^{-1}\cdot\text{kg}^{-1}$. After paramagnetic correction, M_s values reach up to 1052.0 $\mu\text{Am}^2\cdot\text{kg}^{-1}$ while the M_r values range from 49.5 to 118.3 $\mu\text{Am}^2\cdot\text{kg}^{-1}$. The Huty Fm. samples show somewhat higher M values than Mraznica Fm. samples, while the ferro/paramagnetic ratios for both units are rather similar; therefore, the differences in susceptibility (generally higher values in the Huty Fm.) can be explained by a larger content of both ferro- and paramagnetic phases in the Huty Fm.

Additionally, the Huty Fm. samples are characterized by slightly higher mean values of H_{cr} and H_c (28.3 mT and 11.7 mT, respectively) than the Mraznica Fm., which suggests a larger contribution of intermediate- and/or high-coercivity minerals. Some hysteresis loops are characterized by a slightly wasp-waisted shape (e.g., Fig. 3e). This shape of hysteresis curves indicates the occurrence of mixed ferromagnetic assemblages of contrasting coercivities. Relatively high saturation fields can indicate the presence of high coercivity

superparamagnetic minerals (most likely hematite) in these samples (Özdemir & Dunlop 2014).

AMS and AARM characteristics

The magnetic susceptibility (K_m) values in each Mraznica Fm. site were rather similar, ranging from 5.49×10^{-5} to 20.1×10^{-5} [SI] (Fig. 6). The shapes of the AMS ellipsoids calculated for all sites, except site Mz6, are similar and vary from dominantly oblate to triaxial, while the corrected anisotropy degree P_j (Jelínek 1981; Chadima & Jelínek 2008) is relatively low and ranges from 1.02 to 1.055. The Mz6 site is significantly different and is characterized by a prolate to triaxial ellipsoid shape and higher values of the P_j (reaching 1.072).

All sites (Mz1, Mz2, Mz3, Mz4, and Mz5) except one (Mz6) display predominantly oblate to triaxial AMS ellipsoids with magnetic foliation parallel to the bedding plane. Despite such clear bedding-planar AMS fabric these sites also show relatively good grouping of the maximum axes. In the Mz1, Mz3, and Mz4 sites and one subfabric at the Mz2 site, the magnetic lineation is well-grouped and sub-parallel to the bedding strike, that is, oriented NNE–SSW (defined in this publication as lineation type A). In turn, the Mz5 site and one subfabric at the Mz2 site show good grouping of lineation lying in the bedding plane and oriented approximately in an E–W direction, namely normal to the bedding strike (defined as lineation B). Similarly, well clustered and E–W oriented lineation is developed in the Mz6 site, but here the minimum and intermediate susceptibility axes form a girdle perpendicular to the k_{MAX} axes with some tendency towards N–S clustering of k_{MIN} axes.

Susceptibility values for the Huty Fm. are slightly higher than those for the Mraznica Fm., ranging from 8.26×10^{-5} to 33.6×10^{-5} [SI] (Fig. 6). The AMS ellipsoid shape is predominantly oblate and only some specimens in the Ht3 and Ht4 sites exhibit a prolate to triaxial ellipsoid shape. The corrected anisotropy degree usually varies from 1.04 to 1.126. However, specimens with prolate ellipsoid shapes have somewhat lower P_j values (approximately 1.02–1.04).

Specimens from the Ht3 and Ht4 sites which are characterized by triaxial ellipsoid shape (Ht3i, Ht4i; Fig. 6) also display an interchange of minimum and maximum axes orientation and therefore meet the criteria of an inverse magnetic fabric (*sensu* Rochette 1988). In these specimens the k_{MAX}

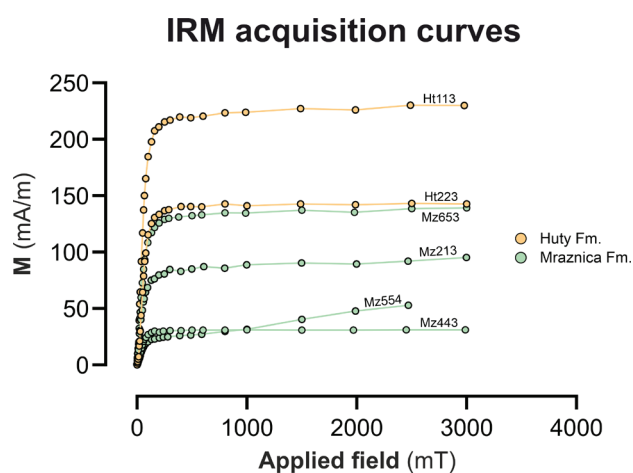


Fig. 5. Isothermal remanent magnetization (IRM) acquisition curves for the Mraznica and Huty fms. samples.

Table 1: IRM component analysis.

Sample	Component 1					Component 2					Component 3				
	Contribution [%]	SIRM [mA/m]	log (B1/2) [mT]	B1/2 [mT]	DP [mT]	Contribution [%]	SIRM [mA/m]	log (B1/2) [mT]	B1/2 [mT]	DP [mT]	Contribution [%]	SIRM [mA/m]	log (B1/2) [mT]	B1/2 [mT]	DP [mT]
Mz213	14.6	15	1.1	12.6	0.3	68.0	70	1.7	50.1	0.4	17.5	18	3.5	3162.3	0.4
Mz443	32.3	10	1.3	20.0	0.3	64.5	20	1.7	52.5	0.3	3.2	1	3.2	1584.9	0.4
Mz554	6.7	4	1.1	12.6	0.4	35.0	21	1.7	50.1	0.4	58.3	35	3.2	1584.9	0.2
Mz653	12.2	17	0.8	6.3	0.2	79.1	110	1.7	50.1	0.3	8.6	12	3.0	1000.0	0.4
Ht113	5.1	12	0.7	5.0	0.3	85.5	200	1.7	49.0	0.3	9.4	22	3.0	1000.0	0.5
Ht223	3.5	5	1.0	10.0	0.5	90.3	130	1.7	53.7	0.3	6.3	9	2.5	316.2	0.4

axes group at the pole to the bedding and the k_{MIN} axes have a NNE–SSW to N–S orientation.

All other specimens from the Huty Fm. (the rest of specimens from the Ht3 and Ht4 sites and all from the Ht1 and Ht2 sites) are characterized by normal magnetic fabric showing bedding parallel foliation with k_{MIN} axes well grouped around the pole to bedding. Specimens with normal magnetic fabric display distinct clustering of magnetic lineation within particular sites. In the Ht2 and Ht3 sites magnetic lineations are well-grouped and show NNE–SSW trend consistent with the bedding strike. In turn, in Ht1 and Ht4n the magnetic lineation is more dispersed and is characterized by an approximately NW–SE orientation.

Anhyseretic Remanence values in the 0–120 mT coercivity window for the Mraznica Fm. range from 8.32×10^{-3} [$A \cdot m^{-1}$] to 140.0×10^{-3} [$A \cdot m^{-1}$]. The shape of the AARM ellipsoid varies quite significantly on both specimen and site level (Fig. 7). The corrected anisotropy degree is usually higher than 1.1 (Fig. 7). There are no significant changes in the shape of the AARM ellipsoid, P_j parameter or the orientation of the axes in the 0×40 mT and 90×120 mT subfabrics (Fig. 7). In the 0×120 mT coercivity window for all sites except Mz6 (Fig. 7) the A_{MAX} axes are well or relatively well grouped and have a sub-vertical (Mz1, Mz2, Mz3, and Mz5) or inclined (Mz4) orientations. In mentioned four sites with sub-vertical lineation the lineation orientations do not seem to be related to the bedding.

Besides AARM lineation most of the sites in the Mraznica Fm. also display a distinct foliation. At the Mz2, Mz3, Mz4, and Mz6 sites, this foliation is sub-vertical, with well grouped NNW–SSE oriented A_{MIN} axes (sites: Mz2, Mz3, and Mz4) to N–S (site: Mz6). The latter Mz6 site, similar to the AMS results, differs from all other sites. Here the magnetic foliation is particularly well defined (mean $T=0.65$) while A_{MAX} and A_{INT} axes form a girdle around the clustered minimum axes with a weak tendency to the horizontal alignment of the maximum axes. In the remaining sites (Mz1 and Mz5) the magnetic foliation is poorly defined ($T=-0.895$, $T=-0.225$, respectively) and A_{MIN} and A_{INT} are generally girdle distributed on a horizontal plane, with some E–W clustering tendency for A_{MIN} axes in the Mz5 site.

Anhyseretic Remanence values for the Huty Fm. (Fig. 8) in the 0–150 mT coercivity window vary from 6.66×10^{-3} [$A \cdot m^{-1}$] to 56.4×10^{-3} [$A \cdot m^{-1}$]. The site-mean AARM ellipsoids (0–150 mT) are oblate to triaxial, while the P_j parameter shows a maximum of 1.208 (Fig. 8). In the 0–150 mT coerci-

Table 2: Results of hysteresis and IRM back-field experiments.

Formation	Site	Sample	Sample values					Ferro/para content [%]	
			M [mAm ² /kg]	Ms [μAm ² /kg]	Mr [μAm ² /kg]	Hc [mT]	Hcr [mT]		
Mraznica	Mz1	Mz14	9.7	391.1	32.0	4.0	16.5	18.6	
		Mz141	12.0	650.1	43.8	4.3	19.2	20.0	
	Mz2	Mz22	16.8	715.3	40.0	5.4	24.1	12.9	
		Mz24	11.8	1070.0	95.0	5.2	19.4	33.8	
	Mz3	Mz312	10.0	189.8	18.0	7.4	20.8	8.0	
		Mz36	12.6	376.6	52.5	8.7	18.8	12.9	
	Mz4	Mz41	9.1	439.0	51.6	9.2	21.8	18.5	
		Mz42	12.6	325.7	43.5	9.8	24.6	10.5	
	Mz5	Mz53	11.3	418.1	38.9	5.1	24.8	14.4	
		Mz55	9.5	478.9	50.1	5.3	18.1	21.8	
		Mz56	11.2	948.8	90.6	7.4	23.7	29.6	
		Mz63	12.0	644.9	56.8	3.3	23.5	20.9	
		Mz65	12.1	798.3	60.4	2.9	22.1	25.9	
	Mean value	–	–	11.6	572.8	51.8	6.0	21.3	19.1
	Standard deviation	–	–	1.9	248.2	20.5	2.2	2.6	7.2
	Huty	Ht1	Ht12	18.3	602.3	83.1	12.8	36.0	11.7
			Ht122	20.6	458.4	70.4	28.2	28.5	4.2
			Ht13	15.4	1052.0	118.3	5.8	26.2	29.9
Ht2		Ht23	29.6	724.7	60.2	9.5	26.9	8.1	
		Ht25	33.4	826.4	64.2	8.8	26.2	7.6	
Ht3		Ht31	16.5	896.0	78.1	8.0	34.8	18.3	
		Ht34	56.4	794.7	49.5	9.5	9.6	3.9	
Ht4		Ht42	22.7	777.5	92.5	10.8	32.3	11.6	
		Ht44	19.3	826.3	89.0	12.0	31.9	17.9	
Mean value		–	–	25.8	773.1	78.4	11.7	28.3	12.6
Standard deviation		–	–	12.2	159.7	19.3	6.2	7.4	7.9

vity window for all examined sites, except Ht4, magnetic foliation lies in a bedding plane, A_{MIN} axes are generally well grouped and are normal to the bedding. In the Ht2 site A_{MAX} axes are dispersed while in the Ht1 and Ht3 sites magnetic lineation has a slight tendency to group in the NW–SE (Ht1; Fig. 8) and NNE–SSW directions (Ht3; Fig. 8). In contrast, at the Ht4 site, the A_{MAX} axes are mostly vertical, while the A_{INT} and A_{MIN} axes form a girdle on the bedding plane.

For the 0–40 mT and 90–150 mT subfabrics, the AARM ellipsoid shape does not change significantly, but the corrected anisotropy degree tends to be higher in the 90–150 mT coercivity window (Fig. 8). The subfabrics detected for the Ht1, Ht2, and Ht3 sites show a tendency to have different preferred A_{MAX} orientations. In the 0–40 mT coercivity window the A_{MAX} tend to group in W–NW directions rather, while in the 90–150 mT coercivity window the NNE–SSW oriented A_{MAX} , parallel to the bedding strike are more common.

Structural analysis

Bedding data were plotted on stereonetts separately for the Mraznica Fm. and CCPB fms. (Fig. 9). Altogether 183 bedding orientations (129 in field, 54 from maps) were measured for the Mraznica Fm. All 21 bedding orientations in the Huty Fm. were measured in the field. Additionally, 45 bedding

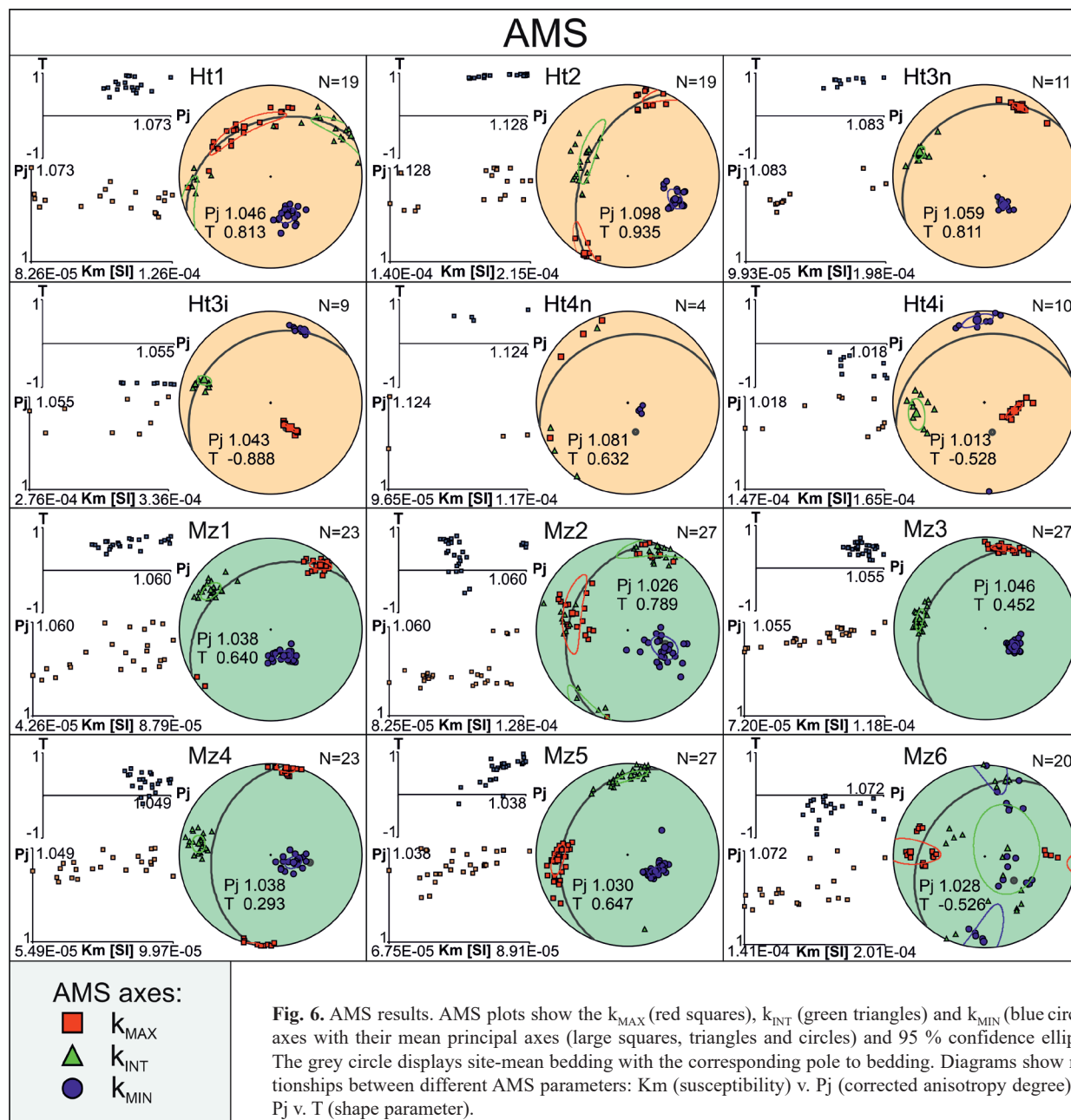


Fig. 6. AMS results. AMS plots show the k_{MAX} (red squares), k_{INT} (green triangles) and k_{MIN} (blue circles) axes with their mean principal axes (large squares, triangles and circles) and 95 % confidence ellipses. The grey circle displays site-mean bedding with the corresponding pole to bedding. Diagrams show relationships between different AMS parameters: Km (susceptibility) v. Pj (corrected anisotropy degree) and Pj v. T (shape parameter).

measurements in the Borové and Zuberec fms. were derived from geological maps (area up to 2 km north of the Mesozoic units). The calculated statistical fold axis of the Mraznica Fm. on the basis of bedding attitude is generally slightly NE-dipping ($020.6/9.4^\circ$), whereas the mean bedding attitude derived from the CCPB data totals $343/35^\circ$.

Discussion

Magnetic mineralogy

The results of petromagnetic experiments allowed us to determine the ferro- and paramagnetic minerals and their contribution to the total susceptibility in the examined

Mraznica Fm. and the Huty Fm. sites. Hysteresis parameters show a relatively homogenous ratio of ferro- and paramagnetics within each of the studied formations (Table 2) with a dominant paramagnetic contribution, which is slightly higher in the case of the Huty Fm. Considering that the lithology of the Mraznica Fm. and Huty Fm. is characterized by a distinct contribution of clay minerals (Borza et al. 1987; Gross et al. 1993; Środoń et al. 2006), phyllosilicates are likely to be the main paramagnetic minerals that govern the susceptibility in both formations. However, some contribution of superparamagnetic magnetite (see paragraph below) to the paramagnetic susceptibility should also be considered. Similar results from carbonate rocks from the Krížna nappe are reported by Gregorová et al. (2009), who suggest that the paramagnetic fraction mostly controls the magnetic susceptibility in these

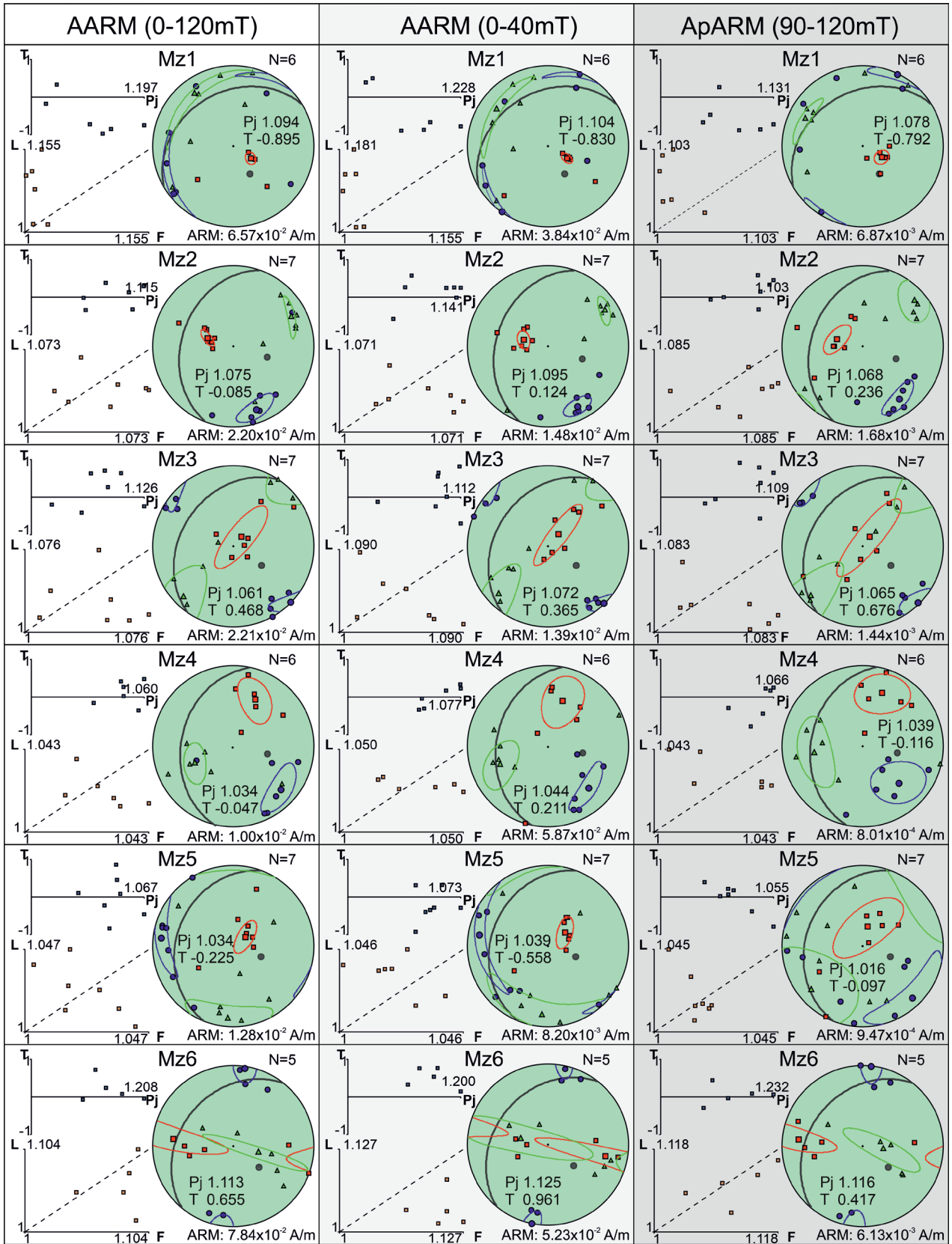


Fig. 7. AARM results for the Mraznica Fm. AARM plots show the A_{MAX} (red squares), A_{INT} (green triangles) and A_{MIN} (blue circles) axes with their mean principal axes (large squares, triangles and circles) and 95 % confidence ellipses. The grey circle displays site-mean bedding with the corresponding pole to bedding. Diagrams show relationships between different AARM parameters: T (shape parameter) v. Pj (corrected anisotropy degree) and L (lineation) v. F (foliation).

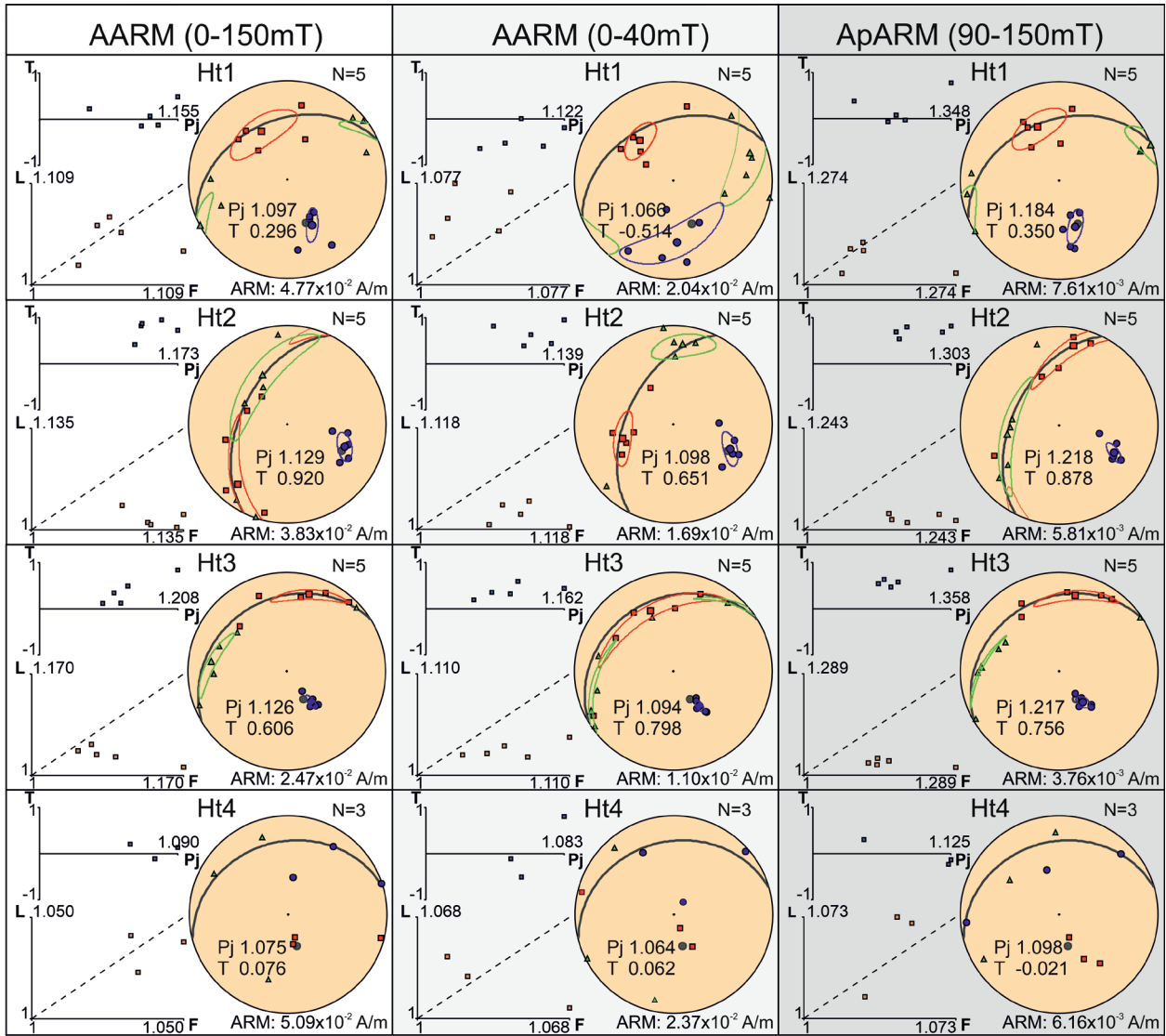


Fig. 8. AARM results for the Hutyna Fm. AARM plots show the A_{MAX} (red squares), A_{INT} (green triangles) and A_{MIN} (blue circles) axes with their mean principal axes (large squares, triangles and circles) and 95 % confidence ellipses. The grey circle shows the site-mean bedding with the corresponding pole to bedding. Diagrams show relationships between different AARM parameters: T (shape parameter) v. Pj (corrected anisotropy degree) and L (lineation) v. F (foliation).

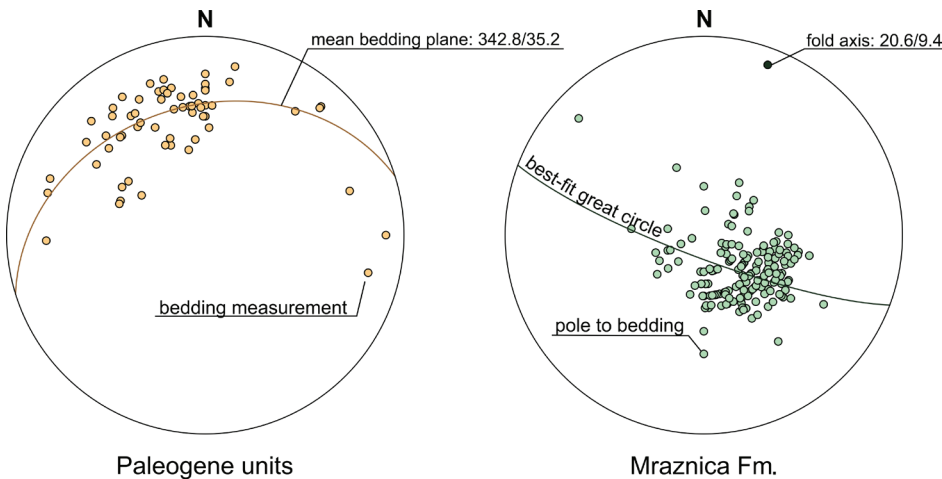


Fig. 9. Stereographic diagrams (lower hemisphere, equal-area projection) display structural data derived from Paleogene units and in the Mraznica Fm.: brown dots show bedding measurements for Paleogene units from which the mean bedding plane orientation was calculated. Green dots display poles to bedding in the Mraznica Fm. The general fold axis for the Mraznica Fm. was calculated using the best-fit great circle method.

units. Our results also correspond well with the results by Grabowski et al. (2009) and Grabowski (1996) from the Strážovské vrchy Mts. and Tatry Mts., respectively. They propose a composite magnetic susceptibility in the Mraznica Fm. originating from paramagnetic and ferromagnetic minerals.

Petromagnetic methods allowed us to distinguish ferromagnetic minerals in rocks of the Mraznica and Huty fms. The results of all applied methods (thermal demagnetization of a three-component IRM, thermal variations in susceptibility, IRM acquisition curves, hysteresis loop, and IRM back-field experiments) indicate the dominance of low-coercivity minerals in both analysed units (Figs. 3, 4, 5). Unblocking temperatures obtained in the thermal demagnetization of a three-component IRM experiment suggest that magnetite is the most common ferromagnetic mineral (Figs. 3, 4). More precise petromagnetic methods (IRM component analysis) allowed us to distinguish two main coercivity windows among the low-coercivity fraction: an intermediate/medium-low coercivity window ($B_{1/2}$ of ~ 50 mT) which covers most of the IRM for both formations and a lowest coercivity window ($B_{1/2}$ of ~ 20 mT) which content is much smaller. We interpret the dominant intermediate/medium-low coercivity component as the presence of SD magnetite possibly with a small contribution of iron sulphides in the Huty Fm. (see paragraph below). Inverse magnetic fabric carried by magnetite in some samples of the Huty Fm. could also support the presence of SD magnetite.

In the Mraznica Fm. we attribute the occurrence of fine-grained SD magnetite to an episode of Late Cretaceous chemical remagnetization widely recognized in carbonate rock of the Križna nappe. The remagnetization mechanism is commonly linked with crystallization of fine-grained magnetite (including SD magnetite and smaller superparamagnetic minerals) related to fluid migrations occurred during early stages of thrusting (Grabowski 1995, 2000; Grabowski et al. 2009; Márton et al. 2016). We cannot exclude the possibility of a second phase of mineral forming related to the burial of Mesozoic nappe units by the CCPB sediments. However, there is no clear evidence for this event. In the case of the Huty Fm. we interpret SD magnetite as diagenetic in origin considering that SD magnetite is commonly formed in organic-rich shales exposed to elevated burial temperatures (Aubourg et al. 2012, 2021; Kars et al. 2012; Zhang et al. 2016; Niezabitowska et al. 2019a, b). The lowest-coercivity of the IRM component occurring in small amounts both in the Mraznica and Huty fms. may represent population of larger, PSD magnetite grains originate during diagenesis and/or in case of the Mraznica Fm. may also represent primary detrital magnetite material. Occurrence of the later detrital magnetite in the Huty Fm. seems to be unlikely as primary magnetite grains dissolve during early diagenesis in organic rich sediments (Canfield & Berner 1987). The latter conclusion is also supported by SEM observation of Madzin et al. (2021) from the CCPB.

The second ferromagnetic phase detected only in the Huty Fm. are ferromagnetic iron sulphides documented by small signal drops occurring at approximately 325 °C during the thermal

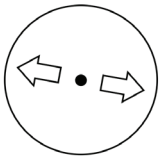
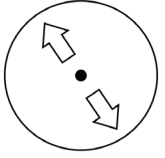
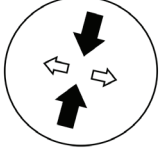
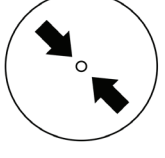
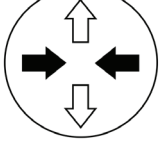
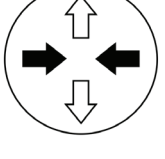
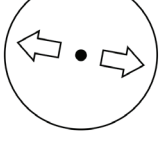
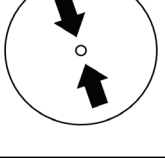
demagnetization of the three-component IRM. The amount of ferromagnetic iron sulphides in these rocks seems relatively low since there is no visible signal drop at 325 °C in the thermal variations of susceptibility measurements. The presence of ferromagnetic iron sulphides is also confirmed by Márton et al. (1999), based on studies of the Huty and Zuberec fms. in CCPB.

We suggest that the observed ferromagnetic iron sulphides phase is most likely pyrrhotite. This mineral commonly occurs in clay- and organic-rich rocks affected by temperatures above 180 °C, although diagenetic pyrrhotite was observed many times in such rocks heated to lower temperatures (e.g., Schoonen & Barnes 1991; Aubourg et al. 2012; Dudzisz et al. 2018). As the sedimentary sequence of CCPB was exposed to the burial temperatures of approximately 100–160 °C (Środoń et al. 2006), the occurrence of pyrrhotite in shales of the Huty Fm. is likely.

The third ferromagnetic mineral documented by petromagnetic experiments is hematite, which was observed in some samples from both the Huty and Mraznica fms. We interpret signal drops at 650 °C in the thermal demagnetization of three-component IRM experiments for two Mraznica Fm. sites (Fig. 3a, b) and the slow, constant increase in magnetic remanence to the highest applied fields in the IRM acquisition curves for all analysed samples (3T; Fig. 5) as indications of the presence of this mineral. Also, some hysteresis loops in the Mraznica Fm. limestones are characterized by slightly wasp-waisted shapes and high saturation fields (Fig. 3e), which could also be linked to a minor hematite contribution (Roberts et al. 1995). We propose that the possible origin of hematite may be detrital, or late diagenetic related to oxidation by fluids with high oxygen content (Lowrie 2007). The current observations, supporting the presence of hematite, agree with previous findings in the Mraznica Fm. reported by Grabowski et al. (2009).

Origin of the AMS and AARM fabrics

Most sites in the Mraznica Fm. (Mz1, Mz2, Mz3, Mz4, Mz5) show dominantly planar AMS fabric with well-defined foliation oriented parallel to bedding (Fig. 6). This indicates that magnetic minerals have mostly retained their original sedimentary-compactional alignment and that their orientations have not been substantially remodelled as a result of later processes. However, apart from such a dominant sedimentary fabric, there is also a distinct magnetic lineation in these sites. In most cases (sites: Mz1, Mz3, Mz4 and one sub-fabric in the Mz2 site) one can observe the lineation defined here as type A, namely NNE–SSW oriented and parallel to both local bedding strike as well as regional statistical fold axis. These observations suggest the tectonic genesis of the lineation type A and its origin related to the compression associated with the Late Cretaceous thrusting processes that led to the folding of Križna nappe rocks (Fig. 10). The origin of the second lineation (type B) detected in the Mraznica Fm. rock and characterized by the E–W orientation is more complicated. We suggest that

Age	Stress orientation	Tectonic regime
Pliocene-Quaternary		EXTENSION
Middle-Late Miocene		TRANSTENSION/EXTENSION
Middle Miocene		
Early Miocene		COMPRESSION/TRANSPRESSION
Late Eocene-Earliest Miocene		
Paleocene-Eocene		TRANSPRESSION
Late Cretaceous Campanian		EXTENSION
Late Cretaceous Cenomanian-Turonian		COMPRESSION

its genesis is also tectonic in origin. The lineation can be associated with localized layer-parallel simple shearing occurring during folding and thrusting, thus parallel to the regional top to the NW tectonic transport (e.g., Averbuch et al. 1992; Szaniawski et al. 2020). Alternatively, such E–W oriented lineation could be related to N–S compression especially since it corresponds to the results obtained from the Mz6 site.

We should note that in the Mz1, Mz2, Mz3, Mz4, and Mz5 sites dominantly planar and bedding parallel AMS fabric with relatively low corrected anisotropy degree corresponds with a composite/intermediate magnetic fabric (sedimentary with some tectonic imprint) according to criteria applied by Parés et al. (1999) and Aubourg et al. (2004). Such magnetic fabrics are typical for sedimentary rocks forming thin-skinned thrust belts (e.g., Dudzisz et al. 2016; Kiss et al. 2016; Szaniawski et al. 2017; Hrouda & Chadima 2019). Different results have been recorded in the Mz6 site. Here, the prolate AMS ellipsoid and specific orientation of principal AMS axes imply locally increased tectonic strain resulting from shortening in the N–S direction. In this site, the primary sedimentary fabric is distinctly overprinted, and the observed magnetic fabric is predominantly tectonic in origin (Fig. 6).

In the Huty Fm., some samples from the Ht3 and Ht4 sites (Ht3i, Ht4i; Fig. 6) showed inverse magnetic results (prolate ellipsoid shaped with an interchange of k_{MAX} and k_{MIN} axes), which we attributed to the occurrence of SD magnetite or Fe-carbonates (Rochette 1988). The rest of the samples display typical magnetic fabric for weakly deformed dark shales, namely strongly oblate AMS ellipsoid with bedding parallel foliation (Aubourg et al. 1991, 1995; Hirt et al. 1995; Dudzisz et al. 2016, 2018; Niezabitowska et al. 2019a, b; 2021). These results reflect good alignment of phyllosilicate plates being predominantly inherited from sedimentary and compactional processes.

The Huty Fm. sites also display feeble lineation. In the Ht2 and Ht3 sites magnetic lineation shows NNE–SSW trend. This could be the result of the currents, as in the vicinity of the Ht2 and Ht3 sites local N to NE paleo-flow directions were reported by Madzin et al. (2021). However, it should be added that different, regional E–W current directions were reported widely from the other parts of CCPB (e.g., Márton et al. 2009; Madzin et al. 2021). On the other hand, in the Ht2 and Ht3 sites k_{MAX} axes are parallel to the local bedding strike and well grouped while reported AMS lineations related to sedimentary processes are typically more dispersed (Parés et al. 1999; Hrouda et al. 2009; Hrouda & Chadima 2019; Stachowska et al. 2020). Therefore, we suggest that lineation in the Ht2 and Ht3 sites is rather of tectonic origin and is related to tectonic strain. In turn, in the case of the Ht1 and Ht4 sites, where the magnetic lineation is dispersed and approximately NW–SE orientated, its origin is unclear – we conclude that it may be both sedimentary and tectonic in origin.

←

Fig. 10. Paleostress field changes from Late Cretaceous to Quaternary (after Pešková et al. 2009 and Králiková et al. 2014b, modified).

The magnetic fabric in AARM measurements for the Mraznica Fm. sites is defined mainly by secondary magnetite. In most of the sites the AARM fabric is characterized by sub-vertical magnetic lineation (Fig. 7). Such specific orientation of AARM lineation could result from preferred orientations of newly formed magnetite crystals controlled by the intersection of a joint system oriented perpendicular to bedding (alternatively preferred crystals orientation could be controlled by the cleavage system). The formation of these joint planes could predate or be the same age as magnetite crystallization. However, this concept is not entirely consistent with the results obtained. In fact, within four sites with sub-vertical (Mz1, Mz2, Mz3, and Mz5) to steeply plunging (Mz4) lineation, the lineation orientations do not seem to be directly related to the bedding. For only two locations (Mz1 and Mz5), the lineation attitude is somewhat similar to perpendicular to the bedding plane. However, in both cases, the bedding poles are noticeably outside the 95 % confidence ellipses for the mean A_{MAX} axis because of folding. In the Mz2 and Mz3 sites, Mz2, Mz3 lineations are subvertical but significantly oblique to the bedding. Therefore, we conclude that the common attitude of lineations in the Mz1, Mz2, Mz3, and Mz5 sites is generally subvertical with some dispersion at the site level and lack of clear correlation with the bedding. In turn, in the case of the Mz4 site, the A_{MAX} axes are moderately well grouped and oriented obliquely between the subvertical position and the bedding strike.

Alternatively, the obtained results may be the effect of transpressive deformations which may result in subvertical tectonic stretching and thus a vertical to steeply plunging lineation was formed (Fossen et al. 1994; Szaniawski et al. 2017). We suggest that deformation linked to Miocene transpression (Ratschbacher et al. 1993; Fodor 1995; Peresson & Decker 1997; Sperner et al. 2002; Marko et al. 2005; Froitzheim et al. 2008) could have reoriented the pre-existing ferromagnetic minerals formed in the Late Cretaceous. In an alternative model, we can assume that subvertical lineation is related to the hypothetical mineralization of a new, second generation of diagenetic magnetite in Early Miocene. It may have been formed at the terminal stages of the burial, during incipient transpression. In such a case the preferred orientation of the newly formed crystals would be determined by the then present stress field, namely subvertical stretching. Such transpressional deformation may not have been strong enough to change the AMS foliation determined by much larger, flat laying paramagnetic phyllosilicate plates being well aligned during sedimentation and compaction.

Most of the Mraznica Fm. sites (Mz2, Mz3, and Mz4) display also distinct sub-vertical magnetic foliation ($340/72.5^\circ$, $314.4/89.2^\circ$ and $311.4/68.5^\circ$, respectively) with NNW–SSE oriented A_{MIN} . We propose that such foliation results from magnetic crystallization within one population of the cleavage system or be the result of shortening in the NNW–SSE direction. In the Mz6 site which also has vertical magnetic foliation ($188.5/86.7^\circ$) A_{MIN} are N–S oriented, while the A_{MAX} and A_{INT} axes form a girdle in the foliation plane which differs from

the most common AARM fabric in the Mraznica Fm. sites. The AARM fabric in the Mz6 site is similar to its AMS fabric and points to a locally increased strain related to N–S-oriented tectonic compression.

In the Huty Fm. the main carriers of AARM fabric are secondary magnetite and possibly pyrrhotite. In most sites (Ht1, Ht2, and Ht3), magnetic foliation follows the bedding plane (Fig. 8). Our interpretation is that the crystallization of secondary magnetite and/or pyrrhotite was strongly controlled by a previously oriented matrix that consisted of flat-lying clay minerals. Generally, the growth of secondary authigenic magnetite is reported to commonly mimic the already existing mineral fabric (Hirt & Gehring 1991; Calvin et al. 2018). Magnetic lineation in sites Ht1, Ht2, and Ht3 is generally NNW–SSE- to N–S-oriented, but its orientation differs slightly for fabrics carried by pyrrhotite (90–150 mT coercivity window) and magnetite (0–40 mT coercivity window). The magnetic lineation defined by pyrrhotite tends to be oriented towards N–NE, while for lower coercivity minerals lineation groups rather in the W–NW directions. In fact, both types of AARM lineation are similar to the two types of AMS lineation defined for the Huty Fm. We suggest that origin of both AARM lineations could be a result of similar processes as in case of the two types of AMS lineation (discussed above). However, in the case of AARM fabric, it is very likely that newly formed ferromagnetic minerals mimic the pre-existed matrix of paramagnetic minerals.

A very different AARM fabric is present in the Ht4 site (Fig. 8) where magnetic lineation is sub-vertical and normal to bedding. This difference seems to be related to lithology as the Ht4 site represents fine-grained sandstones, unlike the remaining shaley sites of the Huty Fm. Here, in sandstones of the Ht4 site, the matrix effect of horizontally aligned clay pallets was undoubtedly weaker than in shales. Hence, other processes controlling magnetic minerals alignment could be more influential. In addition, sandstones have different mechanical properties being more prone to brittle deformations, such as formation of joint network formed in the Miocene (e.g., Boretti-Onyszkiewicz 1968; Ludwiniak 2010). The interpretations presented below correspond to those for the vertical A_{MAX} axes in AARM diagrams for the Mraznica Fm. Crystallization of magnetic minerals with preferred orientations controlled by intersection of such vertical joint system could be one explanation of the subvertical lineation in the Ht4 site. Alternatively, this magnetic fabric could be an effect of Miocene transpression and subvertical stretching – in this model crystallization of magnetic minerals could predate deformations or have the same age as transpression assuming the influence of the stress field on the growth of minerals.

Tectonic interpretation of magnetic data

The most conspicuous results of our studies are the orientations of statistical fold axis and main AMS lineation (lineation type A) from the Mraznica Fm. both interpreted as results of Late Cretaceous compression. They are both NNE-oriented

and slightly plunging. The minor inclination of fold axes and AMS lineation is easily explainable considering Neogene uplift of the asymmetric Chočské vrchy Mts. horst block (see discussion below). However, their general SSW–NNE trend is more difficult to explain as it does not match the expected orientation related to the NW thrusting direction of the Krížna nappe. The later regional direction of the Krížna nappe emplacement is well documented by numerous tectonic–structural studies (Prokešová 1994; Kováč & Bendík 2002; Plašienka 2003; Prokešová et al. 2012) and also is matching with most of the outcomes of magnetic fabric studies reporting E–W to NE–SW magnetic lineations attributed to Late Cretaceous compression (Hrouda & Kahan 1991; Grabowski 1996; Gregorová et al. 2009; Szaniawski et al. 2020). We suggest that the observed aberrant orientations of both the calculated fold axis and AMS lineation result from later deformations, most probably Miocene sinistral transpression well documented in the CCPB in numerous papers (e.g., Fodor 1995; Pešková et al. 2009). We suggest that such transpressional deformations were especially pronounced in the Chočské vrchy Mts. This area constitutes a relatively narrow belt of outcropping Mesozoic strata bounded from the south by fault and interpreted as a regional sinistral transpressional zone related to regional lateral extrusion and uplift of the nearby Tatry Mts. massif as a restraining bend (Sperner et al. 2002). The above magnetic results combined with the sparse structural data set encourage us to speculate on the mechanism of the axis rotation described above. The Chočské vrchy Mts. are bound to the south by the Choč-Subtatic Fault Zone (ENE–WSW-trending). Apart from dip separation along the fault, which drove exhumation, significant sinistral component driven by transpression regime due to far-field of the Eastern Alps tectonic extrusion has been proposed (Peresson & Decker 1997; Sperner et al. 2002; Ludwiniak et al. 2019). Sinistral transpression-related deformation supported counter-clockwise rotation of the fold axis from expected ENE to measured NNE. Transpression-related deformations are probably also responsible for the subvertical lineation in AARM for the Mraznica Fm. and in site Ht4.

Except for the prevailing NNE–SSW-oriented AMS magnetic lineation (type A), a second W–E- to WNW–ESE-oriented magnetic lineation is present in the Mraznica Fm. (lineation type B) and in Ht1 and Ht4 sites in the Huty Fm. The corresponding N–S to NNE–SSW compression could be linked with Middle Miocene compression, so these sites likely document paleostress field rotation (from transpressional to compressional tectonic regime with rotation of principal compressional paleostress axis from NW–SE through N–S to NNE–SSW direction) during the Early and Middle Miocene, as reported by Pešková et al. (2009) in the Upper Eocene to Oligocene and Middle Miocene rocks of the Orava region and by Vojtko et al. (2010) in the Upper Eocene to Oligocene and Mesozoic rocks in the Tatry Mts. and the Spišská Magura Mts. Similar compressional stress most probably led to the formation of sub-vertical AARM foliation (WSW–ENE oriented) observed in the Mraznica Fm.

Bedding analysis revealed that the average dip of the CCPB formations is approximately 30° which was supposed to determine the tilt angle of the whole Chočské vrchy Mts. asymmetric horst. However, this result is not compatible with the very small plunge (~9°) of the Mraznica Fm. fold axis (axes that formed during nappe emplacement are typically sub-horizontal (e.g., Fossen 2010), so we expected that the inclination of the fold axis should reflect the deflection of the entire Chočské vrchy Mts. block during exhumation). One explanation for this situation may be that Paleogene units in the northern part of the Chočské vrchy Mts. could have acquired a distinct dip during sedimentation on a basal slope. In the Late Cretaceous to Early Eocene, the Mesozoic nappes and crystalline basement experienced exhumation; thus, they could probably have formed ridge-like structures dividing smaller Paleogene basins (Kováč et al. 1994, 2016; Kázmér et al. 2003). The deposition on the slope is also supported by conglomerate facies of the transgressive Borové Fm., indicating that an Eocene sea entered the steep rocky shore, yet, this could have likely contributed to the difference between the average Borové Fm. dip and the Mraznica Fm., however, not with deep marine Huty Fm. Hence, the syn-sedimentary factor may be rather excluded.

The second and, in our opinion, more probable interpretation is the model of complex, transpressive uplift of the Chočské vrchy Mts. associated with intensive local fault-block deformations at that time. It differs from what is known about the exhumation of the nearby Tatra Block, which was elevated in the form of rather coherent foreland-tilted horst-blocks. The latter is documented in the Tatry Mts. by corresponding bedding orientations of Triassic autochthonous sedimentary cover and basal parts of the Paleogene sedimentary sequence (Szaniawski et al. 2012).

Conclusions

- Magnetic susceptibility in the Huty and Mraznica fms. rocks is governed predominantly by paramagnetic minerals (phyllosilicates) with a moderate contribution of ferromagnetic minerals (mostly magnetite). Additionally, petromagnetic experiments document the presence of small amounts of other ferromagnetic minerals, such as pyrrhotite and hematite.
- Imparting AARM into three coercivity windows enabled us to characterize different fabrics for magnetite and pyrrhotite windows in the Huty Fm. The pyrrhotite fabric shows a northward-oriented magnetic lineation, which generally coincides with the examined sites' AMS fabric.
- Sub-vertical magnetic lineation present in the AARM fabric of the Mraznica Fm. is related most likely to Miocene transpression and results from magnetite grain reorientation or growing of new minerals under tectonic stress.
- The AMS fabric of the Mraznica and Huty fms. rocks generally display sedimentary fabric characterized by bedding-parallel foliation with a tectonic overprint.

- NNE–SSW-oriented magnetic lineation in almost all Mraznica Fm. and some Huty Fm. sites corresponds well with the calculated fold axis orientation for Krížna nappe folds. Nevertheless, it deflects from the expected orientation of tectonic structures formed during the NW-oriented emplacement of the Krížna nappe. We interpret this difference as a result of deformation related to Miocene transpression along the Choč-Subtatic Fault Zone, which remodelled the primary orientation of Krížna nappe folds formed during nappe displacement.

Acknowledgements: The authors would like to cordially thank the two anonymous Reviewers and the Associate Editor, Rastislav Vojtko, for all comments and suggestions which helped improve the manuscript. A few magnetic and structural results presented in this paper were a part of the Masters dissertation of D. Staneczek. This work was supported by the National Science Centre, Poland (Grant NCN2014/13/B/ST10/01151). All the data are reported in Tables 1–2 and raw data for magnetic analysis used for diagrams can be found at IG PAS Data Portal (https://doi.org/10.25171/InstGeoph_PAS_IGData-ZM-2021-001).

References

- Anczkiewicz A.A., Danišik M. & Środoń J. 2015: Multiple low-temperature thermochronology constraints on exhumation of the Tatra Mountains: New implication for the complex evolution of the Western Carpathians in the Cenozoic. *Tectonics* 34, 2296–2317. <https://doi.org/10.1002/2015TC003952>
- Andrusov D. 1968: Grundriss der Tektonik der nördlichen Karpaten. *Verlag der slowakischen Akademie der Wissenschaften*, Bratislava, 1–188.
- Aubourg C., Rochette P. & Vialon P. 1991: Subtle stretching lineation revealed by magnetic fabric of Callovian-Oxfordian black shales (French Alps). *Tectonophysics* 185, 211–223. [https://doi.org/10.1016/0040-1951\(91\)90445-X](https://doi.org/10.1016/0040-1951(91)90445-X)
- Aubourg C., Rochette P. & Bergmüller F. 1995: Composite magnetic fabric in weakly deformed black shales. *Physics of the Earth and Planetary Interiors* 87, 267–278. [https://doi.org/10.1016/0031-9201\(94\)02962-B](https://doi.org/10.1016/0031-9201(94)02962-B)
- Aubourg C., Smith B., Bakhtari H., Guya N., Eshragi A., Lallemand S., Molinaro M., Brau X. & Delaunay S. 2004: Post-Miocene shortening pictured by magnetic fabric across the Zagros-Makran syntaxis (Iran). In: Special Paper 383: Orogenic Curvature: Integrating Paleomagnetic and Structural Analyses. *Geological Society of America*, 17–40. [https://doi.org/10.1130/0-8137-2383-3\(2004\)383\[17:PSPBMF\]2.0.CO;2](https://doi.org/10.1130/0-8137-2383-3(2004)383[17:PSPBMF]2.0.CO;2)
- Aubourg C., Pozzi J.-P. & Kars M. 2012: Burial, claystones remagnetization and some consequences for magnetostratigraphy. *Geological Society, London, Special Publications* 371, 181–188. <https://doi.org/10.1144/SP371.4>
- Aubourg C., Kars M., Pozzi J.-P., Mazurek M. & Grauby O. 2021: A Magnetic Geothermometer in Moderately Buried Shales. *Minerals* 11, 957. <https://doi.org/10.3390/min11090957>
- Averbuch O., Frizon de Lamotte D. & Kissel C. 1992: Magnetic fabric as a structural indicator of the deformation path within a fold-thrust structure: a test case from the Corbières (NE Pyrenees, France). *Journal of Structural Geology* 14, 461–474. [https://doi.org/10.1016/0191-8141\(92\)90106-7](https://doi.org/10.1016/0191-8141(92)90106-7)
- Bac-Moszaszwili M., Burchart J., Głazek J.F., Iwanow A., Jaroszewski W., Kotański Z., Lefeld J., Mastella L.M., Ozimkowski W. & Roniewicz P. 1979: Geological Map of the Polish Tatra Mountains 1: 30 000. *Wydawnictwa Geologiczne*, Warszawa.
- Boretti-Onyszkiewicz W. 1968: Joints in the Flysch of Western Podhale. *Acta Geologica Polonica* 18, 101–152 (in Polish).
- Borza K., Michalík J. & Vašíček Z. 1987: Lithological, biofacial and geochemical characterization of the Lower Cretaceous pelagic carbonate sequence of Mt. Butkov (Manín Unit, West Carpathians). *Geologický zborník – Geologica Carpathica* 38, 323–348.
- Burchart J. 1972: Fission-track age determinations of accessory apatite from the Tatra Mountains, Poland. *Earth and Planetary Science Letters* 15, 418–422. [https://doi.org/10.1016/0012-821X\(72\)90041-6](https://doi.org/10.1016/0012-821X(72)90041-6)
- Calvin P., Villalain J.J. & Casas-Sainz A.M. 2018: Anisotropic magnetite growth in remagnetized limestones: Tectonic constraints and implications for basin history. *Geology* 46, 751–754. <https://doi.org/10.1130/G45158.1>
- Canfield D.E. & Berner R.A. 1987: Dissolution and pyritization of magnetite in anoxic marine sediments. *Geochimica et Cosmochimica Acta* 51, 645–659. [https://doi.org/10.1016/0016-7037\(87\)90076-7](https://doi.org/10.1016/0016-7037(87)90076-7)
- Castelluccio A., Mazzoli S., Andreucci B., Jankowski L., Szaniawski R. & Zattin M. 2016: Building and exhumation of the Western Carpathians: New constraints from sequentially restored, balanced cross sections integrated with low-temperature thermochronometry. *Tectonics* 35, 2698–2733. <https://doi.org/10.1002/2016TC004190>
- Chadima M. & Hrouda F. 2012: Cureval 8.0.2: Thermomagnetic Curve Analyser for Windows. <https://www.agico.com/text/software/cureval/cureval.php>
- Chadima M. & Jelinek V. 2008: Anisoft 4.2. – Anisotropy data browser. *Contributions to Geophysics and Geodesy* 38, Special Issue, 38–41.
- Csontos L. & Vörös A. 2004: Mesozoic plate tectonic reconstruction of the Carpathian region. *Palaeogeography, Palaeoclimatology, Palaeoecology* 210, 1–56. <https://doi.org/10.1016/j.palaeo.2004.02.033>
- Činčura J. 1990: Characteristics features of Prealpine and Epialpine landmass of the West Carpathians. *Geologický zborník – Geologica Carpathica* 41, 29–38.
- Činčura J. 2002: Paleoalpine paleokarst of the Western Carpathians. In: Proceedings of XVII. Congress of Carpathian-Balkan Geological Association. *Geologica Carpathica* 53, Special Issue. <http://www.geologicacarpatica.com/special-issues/53-2002/>
- Danišik M., Kohút M., Broska I. & Frisch W. 2010: Thermal evolution of the Malá Fatra Mountains (Central Western Carpathians): insights from zircon and apatite fission track thermochronology. *Geologica Carpathica* 61, 19–27. <https://doi.org/10.2478/v10096-009-0041-0>
- Danišik M., Kadlec J., Glotzbach C., Weisheit A., Dunkl I., Kohút M., Evans N.J., Orvošová M. & McDonald B.J. 2011: Tracing metamorphism, exhumation and topographic evolution in orogenic belts by multiple thermochronology: a case study from the Nízke Tatry Mts., Western Carpathians. *Swiss Journal of Geosciences* 104, 285–298. <https://doi.org/10.1007/s00015-011-0060-6>
- Dudzisz K., Szaniawski R., Michalski K. & Manby G. 2016: Applying the anisotropy of magnetic susceptibility technique to the study of the tectonic evolution of the West Spitsbergen Fold-and-Thrust Belt. *Polar Research* 35, 31683. <https://doi.org/10.3402/polar.v35.31683>
- Dudzisz K., Szaniawski R., Michalski K. & Chadima M. 2018: Rock magnetism and magnetic fabric of the Triassic rocks from the West Spitsbergen Fold-and-Thrust Belt and its foreland. *Tectonophysics* 728–729, 104–118. <https://doi.org/10.1016/j.tecto.2018.02.007>

- Fodor L. 1995: From transpression to transtension: Oligocene–Miocene structural evolution of the Vienna basin and the East Alpine–Western Carpathian junction. *Tectonophysics* 242, 151–182. [https://doi.org/10.1016/0040-1951\(94\)00158-6](https://doi.org/10.1016/0040-1951(94)00158-6)
- Fossen H. 2010: Structural Geology. *Cambridge University Press*, 1–463. <https://doi.org/10.1017/CBO9780511777806>
- Fossen H., Tikoff B. & Teyssier C. 1994: Strain modeling of transpressional and transtensional deformation. *Norsk geologisk tidsskrift* 74, 134–145.
- Froitzheim N., Plašienka D. & Schuster R. 2008: Alpine tectonics of the Alps and Western Carpathians. In: McCann T. (Ed.) *The Geology of Central Europe Volume 2: Mesozoic and Cenozoic. The Geological Society of London*, 1141–1232. <https://doi.org/10.1144/CEV2P.6>
- Grabowski J. 1995: New palaeomagnetic data from the Lower Sub-Tatric radiolarites, Upper Jurassic (Western Tatra Mts.). *Geological Quarterly* 39, 61–74.
- Grabowski J. 1996: Magnetic fabric of the Upper Jurassic sediments, Krížna Unit, Tatra Mts., Poland. *Geologica Carpathica* 47, 331–337.
- Grabowski J. 1997: Paleomagnetic results from the cover (High-Tatric) unit and nummulitic Eocene in the Tatra Mts (Central West Carpathians, Poland) and their tectonic implications. *Annales Societatis Geologorum Poloniae* 67, 13–23.
- Grabowski J. 2000: Palaeo- and rock magnetism of mesozoic carbonate rocks in the sub-tatric series (Central West Carpathians) – palaeotectonic implications. *Polish Geological Institute Special Papers* 5, 1–88.
- Grabowski J., Michalik J., Szaniawski R. & Grottek I. 2009: Syn-thrusting remagnetization of the Krížna nappe: high resolution palaeo- and rock magnetic study in the Strážovce section, Strážovské vrchy Mts, Central West Carpathians (Slovakia). *Acta Geologica Polonica* 59, 137–155.
- Gregorová D., Hrouda F. & Kohút M. 2009: Magnetic fabric of granitic composite pluton of the Veľká Fatra Mountains (Western Carpathians, Slovakia): A Variscan remnant within the Alpine edifice? *Geodinamica Acta* 22, 57–72. <https://doi.org/10.3166/ga.22.57-72>
- Gross P., Köhler E. (Eds.), Biely A., Franko O., Hanzel V., Hricko J., Kupčo G., Papšová J., Priechedská Z., Szalαιοová V., Snopková P., Stránska M., Vaškovský I. & Zbořil E. 1980: Geology of Liptovská kotlina Depression. *Geologický ústav Dionýza Štúra*, Bratislava, 1–242.
- Gross P., Köhler E. & Samuel O. 1984: A new lithostratigraphical division of the Inner-Carpathian Paleogene. *Geologické Práce, Správy* 81, 103–117.
- Gross P., Köhler E., Haško J., Halouzka R., Mello J. & Nagy A. 1993: Geology of the southern and eastern Orava. *Štátny Geologický Ústav Dionýza Štúra*, Bratislava, 1–319 (in Slovak).
- Gross P., Filo I., Halouzka R., Haško J., Havrila M., Kováč P., Maglay J., Mello J. & Nagy A. 1994: Geological map of southern and eastern part of Orava 1:50 000. *Ministerstvo Životného Prostredia – Geologický Ústav Dionýza Štúra*, Bratislava (in Slovak).
- Havrila M. 2011: Hronicum: paleogeography and stratigraphy (Upper Pelson–Tuvalian), tectonic individualization and structure. *Geologické Práce, Správy* 117, 7–103.
- Hirt A.M. & Gehring A.U. 1991: Thermal alteration of the magnetic mineralogy in ferruginous rocks. *Journal of Geophysical Research: Solid Earth* 96, 9947–9953. <https://doi.org/10.1029/91JB00573>
- Hirt A.M., Evans K.F. & Engelder T. 1995: Correlation between magnetic anisotropy and fabric for Devonian shales on the Appalachian Plateau. *Tectonophysics*, 30 Years of Tectonophysics, a Special Volume in Honour of Gerhard Oertel 247, 121–132. [https://doi.org/10.1016/0040-1951\(94\)00176-A](https://doi.org/10.1016/0040-1951(94)00176-A)
- Hrouda F. 1983: Fabric implications of magnetic anisotropy measurements of rocks of the Malé Karpaty (Little Carpathians) Mts. (SW Slovakia). *Annuaire Inst. Geol. Geophys.* 63, 57–61.
- Hrouda F. 1986: The magnetic fabric of sedimentary rocks of the Malé Karpaty Mts. and its tectonic implications. *Sborník geologických věd* 20, 165–167.
- Hrouda F. & Chadima M. 2019: Examples of tectonic overprints of magnetic fabrics in rocks of the Bohemian Massif and Western Carpathians. *International Journal of Earth Sciences (Geol Rundsch)* 109, 1321–1336. <https://doi.org/10.1007/s00531-019-01786-8>
- Hrouda F. & Hanák J. 1990: Magnetic fabric of sedimentary formations of the Strazovske vrchy Mts., sedimentological and tectonic implications. *Sborník geologických věd, Užitá geofyzika* 24, 71–102.
- Hrouda F. & Kahan Š. 1991: The magnetic fabric relationship between sedimentary and basement nappes in the High Tatra Mountains, N. Slovakia. *Journal of Structural Geology* 13, 431–442. [https://doi.org/10.1016/0191-8141\(91\)90016-C](https://doi.org/10.1016/0191-8141(91)90016-C)
- Hrouda F. & Potfaj M. 1993: Deformation of sediments in the post-orogenic Intra-Carpathian Paleogene Basin as indicated by magnetic anisotropy. *Tectonophysics* 224, 425–434. [https://doi.org/10.1016/0040-1951\(93\)90042-1](https://doi.org/10.1016/0040-1951(93)90042-1)
- Hrouda F. & Vozár J. 1995: Tectonic interaction between the Internides and Centralides of the Inner West Carpathians, as indicated by magnetic anisotropy. *Journal of the Czech Geological Society* 40, 67.
- Hrouda F., Stephenson A. & Woltär L. 1983: On the standardization of measurements of the anisotropy of magnetic susceptibility. *Physics of the Earth and Planetary Interiors* 32, 203–208. [https://doi.org/10.1016/0031-9201\(83\)90125-5](https://doi.org/10.1016/0031-9201(83)90125-5)
- Hrouda F., Jelínek V. & Zapletal K. 1997: Refined technique for susceptibility resolution into ferromagnetic and paramagnetic components based on susceptibility temperature-variation measurement. *Geophysical Journal International* 129, 715–719. <https://doi.org/10.1111/j.1365-246X.1997.tb04506.x>
- Hrouda F., Putiš M. & Madarás J. 2002: The Alpine overprints of the magnetic fabrics in the basement and cover rocks of the Veporic Unit (Western Carpathians, Slovakia). *Tectonophysics* 359, 271–288.
- Hrouda F., Krejčí O., Potfaj M. & Stránil Z. 2009: Magnetic fabric and weak deformation in sandstones of accretionary prisms of the Flysch and Klippen Belts of the Western Carpathians: Mostly offscraping indicated. *Tectonophysics* 479, 254–270. <https://doi.org/10.1016/j.tecto.2009.08.016>
- Hrouda F., Gilder S., Wack M. & Ježek J. 2018: Diverse response of paramagnetic and ferromagnetic minerals to deformation from Intra-Carpathian Palaeogene sedimentary rocks: Comparison of magnetic susceptibility and magnetic remanence anisotropies. *Journal of Structural Geology* 113, 217–224. <https://doi.org/10.1016/j.jsg.2018.06.001>
- Jelínek V. 1977: The statistical theory of measuring anisotropy of magnetic susceptibility of rocks and its application. *Geofyzika*, Brno, 1–88.
- Jelínek V. 1981: Characterization of the magnetic fabric of rocks. *Tectonophysics* 79, T63–T67. [https://doi.org/10.1016/0040-1951\(81\)90110-4](https://doi.org/10.1016/0040-1951(81)90110-4)
- Józsa Š., Boorová D. & Filo I. 2016: Aptian planktonic foraminiferal biostratigraphy and smaller benthic foraminifera from the Párnica Formation (Choč Mts., Western Carpathians). *Acta Geologica Slovaca* 8, 15–26.
- Jurewicz E. 2005: Geodynamic evolution of the Tatra Mts. and the Pieniny Klippen Belt (Western Carpathians): problems and comments. *Acta Geologica Polonica* 55, 295–338.
- Jurewicz E. 2012: Nappe-thrusting processes in the Tatra Mts. *Przeгляд Geologiczny* 60, 432–441 (in Polish).
- Kars M., Aubourg C., Pozzi J.-P. & Janots D. 2012: Continuous production of nanosized magnetite through low grade burial. *Geochemistry, Geophysics, Geosystems* 13. <https://doi.org/10.1029/2012GC004104>
- Kázmér M., Dunkl I., Frisch W., Kuhlemann J. & Ozsvárt P. 2003: The Palaeogene forearc basin of the Eastern Alps and Western Carpathians: subduction erosion and basin evolution. *Journal of the Geological Society* 160, 413–428. <https://doi.org/10.1144/0016-764902-041>

- Kiss D., Márton Péterné Szalay E. & Tokarski A.K. 2016: An integrated paleomagnetic and magnetic anisotropy study of the Oligocene flysch from the Dukla nappe, Outer Western Carpathians, Poland. *Geologica Carpathica* 67, 595–605. <https://doi.org/10.1515/geoca-2016-0037>
- Kohút M., Kovach V., Kotov A., Salnikova E. & Savatenkov V. 1999: Sr and Nd isotope geochemistry of Hercynian granitic rocks from the Western Carpathians – Implications for granite genesis and crustal evolution. *Geologica Carpathica* 50, 477–487.
- Kováč M., Král J., Márton E., Plašienka D. & Uher, P. 1994: Alpine uplift history of the Central Western Carpathians: geochronological, paleomagnetic, sedimentary and structural data. *Geologica Carpathica* 45, 83–96.
- Kováč M., Plašienka D., Soták J., Vojtko R., Oszczytko N., Less G., Čosović V., Fügenschuh B. & Králiková S. 2016: Paleogene palaeogeography and basin evolution of the Western Carpathians, Northern Pannonian domain and adjoining areas. *Global and Planetary Change* 140, 9–27. <https://doi.org/10.1016/j.gloplacha.2016.03.007>
- Kováč M., Márton E., Klučiar T. & Vojtko R. 2018: Miocene basin opening in relation to the north-eastward tectonic extrusion of the ALCAPA Mega-Unit. *Geologica Carpathica* 69, 254–263. <https://doi.org/10.1515/geoca-2018-0015>
- Kováč P. & Bendík A. 2002: Structural analysis of Adnet limestones at Zvolen–Donovaly. *Mineralia Slovaca* 34, 207–210.
- Kováč P. & Filo I., 1992: Structural interpretation of the Choč nappe outliers of the Chočské vrchy Mts. *Mineralia Slovaca* 24, 39–44.
- Král J. 1977: Fission track ages of apatites from some granitoid rocks in West Carpathians. *Geologický zborník – Geologica Carpathica* 28, 269–276.
- Králiková S., Vojtko R., Andriessen P., Kováč M., Fügenschuh B., Hók J. & Minár J. 2014a: Late Cretaceous–Cenozoic thermal evolution of the northern part of the Central Western Carpathians (Slovakia): revealed by zircon and apatite fission track thermochronology. *Tectonophysics* 615–616, 142–153. <https://doi.org/10.1016/j.tecto.2014.01.002>
- Králiková S., Vojtko R., Sliva U., Minár J., Fügenschuh B., Kováč M. & Hók J. 2014b: Cretaceous–Quaternary tectonic evolution of the Tatra Mts (Western Carpathians): constraints from structural, sedimentary, geomorphological, and fission track data. *Geologica Carpathica* 65, 307–326. <https://doi.org/10.2478/geoca-2014-0021>
- Králiková S., Vojtko R., Hók J., Fügenschuh B. & Kováč M. 2016: Low-temperature constraints on the Alpine thermal evolution of the Western Carpathian basement rock complexes. *Journal of Structural Geology* 91, 144–160. <https://doi.org/10.1016/j.jsg.2016.09.006>
- Kruczyk J., Kaździako–Hofmokl M., Lefeld J., Pagač P. & Tunyi I. 1992: Paleomagnetism of Jurassic sediments as evidence for oroclinal bending of the Inner West Carpathians. *Tectonophysics* 206, 315–324. [https://doi.org/10.1016/0040-1951\(92\)90383-H](https://doi.org/10.1016/0040-1951(92)90383-H)
- Kruiver P.P., Dekkers M.J. & Heslop D. 2001: Quantification of magnetic coercivity components by the analysis of acquisition curves of isothermal remanent magnetisation. *Earth and Planetary Science Letters* 189, 269–276. [https://doi.org/10.1016/S0012-821X\(01\)00367-3](https://doi.org/10.1016/S0012-821X(01)00367-3)
- Lexa J., Bezák V., Elečko M., Mello J., Polák M., Potfaj M., Vozár J., Schnabel G.W., Pálenský P., Császár G., Ryško W. & Mackiv B. 2000: Geological map of Western Carpathians and adjacent areas 1:500 000. Correlation Tables of Lithostratigraphic Units. *Geological Survey of Slovak Republic*, Bratislava.
- Lowrie W. 1990: Identification of ferromagnetic minerals in a rock by coercivity and unblocking temperature properties. *Geophysical Research Letters* 17, 159–162. <https://doi.org/10.1029/GL017i002p00159>
- Lowrie W. 2007: Fundamentals of Geophysics. *Cambridge University Press*, Cambridge, 1–381.
- Ludwiniak M. 2010: Multi-stage development of the joint network in the flysch rocks of western Podhale (Inner Western Carpathians, Poland). *Acta Geologica Polonica* 60, 283–316.
- Ludwiniak M. & Rubinkiewicz J. 2006: Fracture and fault development in Werfenian quartzitic sandstones – A case study from the autochthonous cover of the Tatra Mts.(in Polish). *Przegląd Geologiczny* 54, 173.
- Ludwiniak M., Śmigieński M., Kowalczyk S., Łoziński M., Czarniecka U. & Lewińska L. 2019: The intramontane Orava Basin – evidence of large-scale Miocene to Quaternary sinistral wrenching in the Alpine-Carpathian-Pannonian area. *Acta Geologica Polonica* 69, 339–386. <https://doi.org/10.24425/aggp.2019.126449>
- Madzin J., Márton E., Starek D. & Mikuš T. 2021: Magnetic fabrics in the turbidite deposits of the Central Carpathian Paleogene Basin in relation to sedimentary and tectonic fabric elements. *Geologica Carpathica* 72, 134–154. <https://doi.org/10.31577/GeolCarp.72.2.4>
- Marko F., Vojtko R., Plašienka D., Sliva L., Jablonský J., Reichwalder P. & Starek D. 2005: A contribution to the tectonics of the Periklappen zone near Zázrivá (Western Carpathians). *Slovak Geological Magazine* 11, 37–43.
- Mazzoli S., Szaniawski R., Mittiga F., Ascione A. & Capalbo A. 2012: Tectonic evolution of Pliocene–Pleistocene wedge-top basins of the southern Apennines: new constraints from magnetic fabric analysis. *Canadian Journal of Earth Sciences* 49, 492–509.
- Márton E., Mastella L. & Tokarski A.K. 1999: Large counterclockwise rotation of the Inner West Carpathian Paleogene Flysch—Evidence from paleomagnetic investigations of the Podhale Flysch (Poland). *Physics and Chemistry of the Earth, Part A: Solid Earth and Geodesy* 24, 645–649. [https://doi.org/10.1016/S1464-1895\(99\)00094-0](https://doi.org/10.1016/S1464-1895(99)00094-0)
- Márton E., Jeleńska M., Tokarski A.K., Soták J., Kováč M. & Spišák J. 2009: Current-independent paleomagnetic declinations in flysch basins: a case study from the Inner Carpathians. *Geodinamica Acta* 22, 73–82. <https://doi.org/10.3166/ga.22.73-82>
- Márton E., Grabowski J., Tokarski A.K. & Tunyi I. 2016: Palaeomagnetic results from the fold and thrust belt of the Western Carpathians: an overview. *Geological Society, London, Special Publications* 425, 7–36. <https://doi.org/10.1144/SP425.1>
- Niezabitowska D.K., Szaniawski R. & Jackson M. 2019a: Magnetic mineral assemblage as a potential indicator of depositional environment in gas-bearing Silurian shales from Northern Poland. *Geophysical Journal International* 218, 1442–1455. <https://doi.org/10.1093/gji/ggz229>
- Niezabitowska D.K., Szaniawski R., Roszkowska-Remin J. & Gasiński A. 2019b: Magnetic Anisotropy in Silurian Gas-Bearing Shale Rocks from the Pomerania Region (Northern Poland). *Journal of Geophysical Research: Solid Earth* 124, 5–25. <https://doi.org/10.1029/2018JB016374>
- Niezabitowska D.K., Roszkowska-Remin J., Szaniawski R. & Derkowski A. 2021: Magnetic susceptibility variations in lower Paleozoic shales of the western Baltic Basin (northern Poland): A tool for regional stratigraphic correlations and the decoding of paleoenvironmental changes. *AAPG Bulletin* 105, 987–1007. <https://doi.org/10.1306/12092019183>
- Özdemir Ö. & Dunlop D.J. 2014: Hysteresis and coercivity of hematite. *Journal of Geophysical Research: Solid Earth* 119, 2582–2594. <https://doi.org/10.1002/2013JB010739>
- Parés J.M. 2015: Sixty years of anisotropy of magnetic susceptibility in deformed sedimentary rocks. *Frontiers in Earth Science* 3. <https://doi.org/10.3389/feart.2015.00004>
- Parés J.M., van der Pluijm B.A. & Dinarès-Turell J. 1999: Evolution of magnetic fabrics during incipient deformation of mudrocks (Pyrenees, northern Spain). *Tectonophysics* 307, 1–14. [https://doi.org/10.1016/S0040-1951\(99\)00115-8](https://doi.org/10.1016/S0040-1951(99)00115-8)
- Peresson H. & Decker K. 1997: Far-field effects of Late Miocene subduction in the Eastern Carpathians: E-W compression and inversion of structures in the Alpines-Carpathian-Pannonian region. *Tectonics* 16, 38–56. <https://doi.org/10.1029/96TC02730>
- Pešková I., Vojtko R., Starek D. & Sliva L. 2009: Late Eocene to Quaternary deformation and stress field evolution of the Orava region (Western Carpathians). *Acta Geologica Polonica* 59, 73–91.

- Petrík I. & Kohút M. 1997: The evolution of granitoid magmatism during the Hercynian orogen in the Western Carpathians. In: Grecula P., Hovorka D. & Putiš M. (Eds.): Geological Evolution of the Western Carpathians. *Mineralia Slovaca - Monograph*, Bratislava, 235–252.
- Plašienka D. 1997: Cretaceous tectonochronology of the Central Western Carpathians (Slovakia). *Geologica Carpathica* 48, 99–111.
- Plašienka D. 2002: Origin and growth of the Western Carpathian orogenic wedge during the Mesozoic. *Geologica Carpathica* 53, Special Issue. <http://www.geologicacarpathica.com/special-issues/53-2002/>
- Plašienka D. 2003: Development of basement-involved fold and thrust structures exemplified by the Tatric–Fatric–Veporic nappe system of the Western Carpathians (Slovakia). *Geodinamica Acta* 16, 21–38. [https://doi.org/10.1016/S0985-3111\(02\)00003-7](https://doi.org/10.1016/S0985-3111(02)00003-7)
- Plašienka D. 2018: Continuity and Episodicity in the Early Alpine Tectonic Evolution of the Western Carpathians: How Large-Scale Processes Are Expressed by the Orogenic Architecture and Rock Record Data. *Tectonics* 37, 2029–2079. <https://doi.org/10.1029/2017TC004779>
- Plašienka D. & Prokešová R. 1996: Towards an evolutionary tectonic model of the Križna cover nappe (Western Carpathians, Slovakia). *Slovak Geological Magazine* 3, 279–286.
- Plašienka D., Grecula P., Putiš M., Hovorka D. & Kováč M. 1997: Evolution and structure of the Western Carpathians: an overview. In: Grecula P., Hovorka D. & Putiš M. (Eds.): Geological Evolution of the Western Carpathians. *Mineralia Slovaca - Monograph*, Bratislava, 1–24.
- Prokešová R. 1994: Structural analysis of the Križna nappe in its near-root and superficial position. *Mineralia Slovaca* 26, 347–354.
- Prokešová R., Plašienka D. & Milovský R. 2012: Structural pattern and emplacement mechanisms of the Križna cover nappe (Central Western Carpathians). *Geologica Carpathica* 63, 13–32. <https://doi.org/10.2478/v10096-012-0001-y>
- Ramsay J.G. & Huber M.I. 1987: The Techniques of Modern Structural Geology. Volume 2: Folds and Fractures. *Academic Press*, London, 1–381.
- Ratschbacher L., Linzer H.G., Moser F., Strusievcz R.O., Bedeleian H., Har N. & Mogoş P.A. 1993: Cretaceous to Miocene thrusting and wrenching along the central south Carpathians due to a corner effect during collision and orocline formation. *Tectonics* 12, 855–873. <https://doi.org/10.1029/93TC00232>
- Roberts A.P., Cui Y. & Verosub K.L. 1995: Wasp-waisted hysteresis loops: Mineral magnetic characteristics and discrimination of components in mixed magnetic systems. *Journal of Geophysical Research: Solid Earth* 100, 17909–17924. <https://doi.org/10.1029/95JB00672>
- Rochette P. 1988: Inverse magnetic fabric in carbonate-bearing rocks. *Earth and Planetary Science Letters* 90, 229–237. [https://doi.org/10.1016/0012-821X\(88\)90103-3](https://doi.org/10.1016/0012-821X(88)90103-3)
- Royden L.H. & Báldi T. 1988: Early Cenozoic Tectonics and Paleogeography of the Pannonian and Surrounding Regions. In: Royden L.H. & Horváth F. (Eds.): The Pannonian Basin: A Study in Basin Evolution. *AAPG* 45. <https://doi.org/10.1306/M45474C1>
- Schoonen M.A.A. & Barnes H.L. 1991: Mechanisms of pyrite and marcasite formation from solution: III. Hydrothermal processes. *Geochimica et Cosmochimica Acta* 55, 3491–3504. [https://doi.org/10.1016/0016-7037\(91\)90050-F](https://doi.org/10.1016/0016-7037(91)90050-F)
- Sentpetery M. 2011: South-vergent structures observed in the western part of the Krivánska Fatra Mts. (Central Western Carpathians). *Acta Geologica Slovaca* 3, 123–129.
- Soták J., Pereszlenyi M., Marschalko R., Milicka J. & Starek D. 2001: Sedimentology and hydrocarbon habitat of the submarine-fan deposits of the Central Carpathian Paleogene Basin (NE Slovakia). *Marine and Petroleum Geology* 18, 87–114. [https://doi.org/10.1016/S0264-8172\(00\)00047-7](https://doi.org/10.1016/S0264-8172(00)00047-7)
- Sperner B., Ratschbacher L. & Nemčok M. 2002: Interplay between subduction retreat and lateral extrusion: Tectonics of the Western Carpathians. *Tectonics* 21, 1-1–1-24. <https://doi.org/10.1029/2001TC901028>
- Šrodoň J., Kotarba M., Biroň A., Such P., Clauer N. & Wójtowicz A. 2006: Diagenetic history of the Podhale-Orava Basin and the underlying Tatra sedimentary structural units (Western Carpathians): evidence from XRD and K-Ar of illite-smectite. *Clay Minerals* 41, 751–774. <https://doi.org/10.1180/0009855064130217>
- Stachowska A., Łoziński M., Śmigielski M., Wysocka A., Jankowski L. & Ziólkowski P. 2020: Anisotropy of magnetic susceptibility as an indicator for palaeocurrent analysis in folded turbidites (Outer Western Carpathians, Poland). *Sedimentology* 67, 3783–3808. <https://doi.org/10.1111/sed.12770>
- Starek D. 2001: Sedimentology and paleodynamics of the Paleogene formations of the Central Western Carpathians. *Slovak Academy of Sciences*, Bratislava, 1–152.
- Starek D., Andreyeva-Grigorovich A.S. & Soták J. 2000: Suprafan deposits of the Biely Potok Fm. in the Orava region: sedimentary facies and nannoplankton distribution. *Slovak Geological Magazine* 6, 188–190.
- Szaniawski R., Ludwiniak M. & Rubinkiewicz J. 2012: Minor counterclockwise rotation of the Tatra Mountains (Central Western Carpathians) as derived from paleomagnetic results achieved in hematite-bearing Lower Triassic sandstones. *Tectonophysics* 560–561, 51–61. <https://doi.org/10.1016/j.tecto.2012.06.027>
- Szaniawski R., Mazzoli S. & Jankowski L. 2017: Controls of structural inheritance on orogenic curvature and foreland basin sedimentation: Insights from the Przemysł area, Western Carpathians. *Journal of Structural Geology* 103, 137–150. <https://doi.org/10.1016/j.jsg.2017.09.004>
- Szaniawski R., Ludwiniak M., Mazzoli S., Szczygiel J. & Jankowski L. 2020: Paleomagnetic and magnetic fabric data from Lower Triassic redbeds of the Central Western Carpathians: new constraints on the paleogeographic and tectonic evolution of the Carpathian region. *Journal of the Geological Society* 177, 509–522. <https://doi.org/10.1144/jgs2018-232>
- Tari G., Báldi T. & Báldi-Beke M. 1993: Paleogene retroarc flexural basin beneath the Neogene Pannonian Basin: A geodynamic model. In: The origin of sedimentary basins: Inferences from quantitative modelling and basin analysis. *Tectonophysics* 226, 433–455. [https://doi.org/10.1016/0040-1951\(93\)90131-3](https://doi.org/10.1016/0040-1951(93)90131-3)
- Vojtko R., Tokárová E., Sliva L. & Pešková I. 2010: Reconstruction of Cenozoic paleostress fields and revised tectonic history in the northern part of the Central Western Carpathians (the Spišská Magura and Východné Tatry Mountains). *Geologica Carpathica* 61, 211–225. <https://doi.org/10.2478/v10096-010-0012-5>
- Vojtko R., Králiková S., Jeřábek P., Schuster R., Danišík M., Fügen-schuh B., Minár J. & Madarás J. 2016: Geochronological evidence for the Alpine tectono-thermal evolution of the Veporic Unit (Western Carpathians, Slovakia). *Tectonophysics* 666, 48–65. <https://doi.org/10.1016/j.tecto.2015.10.014>
- Westwalewicz-Mogilska E. 1986: A new look on the origin of the Podhale Flysch sediments. *Przegląd Geologiczny* 34, 690–698.
- Zhang Y., Jia D., Yin H., Liu M., Xie W., Wei G. & Li Y. 2016: Remagnetization of lower Silurian black shale and insights into shale gas in the Sichuan Basin, south China. *Journal of Geophysical Research: Solid Earth* 121, 491–505. <https://doi.org/10.1002/2015JB012502>

Appendix

Sample localities

Sampling site	Geographic coordinates	Short description of the sampling site	Number of hand samples
Mz1	49°09'16.0"N 19°22'22.8"E	Outcrop along a road from Lúčky to Vyšný Kubín, Mraznica Fm.	6
Mz2	49°08'39.6"N 19°23'38.2"E	Outcrop along a forest road on the southern slopes of Magura hill, Mraznica Fm.	7
Mz3	49°06'06.2"N 19°25'47.3"E	Outcrop in the southern part of the Sestrč valley, Mraznica Fm.	7
Mz4	49°09'49.4"N 19°25'55.0"E	Large outcrop along a road in the Sestrč valley, Mraznica Fm.	6
Mz5	49°07'41.0"N 19°17'41.2"E	Outcrop along a road on the western slopes of Hulín hill, Mraznica Fm.	7
Mz6	49°8'44.556"N 19°21'20.1456"E	Outcrop along a road on the slopes of Bukov hill; Mraznica Fm.	5
Ht1	49°12'33.336"N 19°32'56.276"E	Outcrop at the crossroad in Huty village; Huty Fm.	5
Ht2	49°12'16.704"N 19°31'48.3348"E	Outcrop in Ráztocký stream near Jóbova Ráztoka settlement; Huty Fm.	5
Ht3	49°12'48.6288"N 19°33'20.3472"E	Outcrop along Kvačianka stream near the cemetery in Huty village; Huty Fm.	5
Ht4	49°10'45.5124"N 19°28'6.7152"E	Outcrop at a forest crossroad on the northern slopes of Lomné hill, near Malatiná village; Huty Fm.	4